Calculation of two-photon processes in hydrogen with an L^2 basis

John T. Broad
Fakultät für Chemie, Universität Bielefeld, D-4800 Bielefeld, Federal Republic of Germany
(Received 1 June 1984)

A new method for calculating atomic multiphoton processes is presented here with application to two-photon processes in atomic hydrogen. The L^2-basis-set approach exploits explicit expansion of the Coulomb radial function and resolvent in terms of Pollaczek polynomials and functions to achieve compact expressions for two-photon radial transition amplitudes. This allows efficient calculation of the Bethe logarithm even for highly excited hydrogenic states and two-photon ionization amplitudes near and above the one-photon ionization threshold. Above the one-photon threshold, the complete-basis limit of the highly oscillatory amplitude is computed by applying the epsilon algorithm carefully to a sequence generated from only 10—15 basis functions. The approach is extended below the one-photon threshold by splitting the transition amplitude into a sum of two formally divergent but geometriclike series, whose analytic continuation is realized by the epsilon algorithm to yield a clearly defined and efficient interpolation between the resonances at highly excited Rydberg states. This suggests a new L^2-basis formulation of the quantum-defect method. The extension to complex basis functions and many-electron atoms in strong fields is discussed.

I. INTRODUCTION

The desire to extend the basis-set methods so successful in quantum chemistry in calculating the properties of bound systems to ionizing and reactive processes has motivated the development of a variety of square-integrable- (L^2-) basis formulations of time-independent scattering theory. When, as is usually true, the systems of interest behave asymptotically as two, or perhaps three, fragments scattering, the advantages of such an approach are evident, for the really difficult problem of describing the structure of the fragments accurately enough can be tackled directly with basis-set methods and the results coupled to and projected on the scattering continuum in a transparent fashion. It is, moreover, not surprising that L^2-basis methods have been applied with most success to resonances and photoionization, which involve the transition from bound states to the continuum.

The challenge to extract full scattering information from a discretization of the appropriate Hamilton operator obtained by truncation of an L^2 basis of a Hilbert space demanded the development of a thorough mathematical understanding of the continuum in function space. While the now well-established concept of pseudostates[1–3] and the techniques of equivalent quadrature[3–10] and Stieltjes imaging[8,11] exploit the discretization directly as interpolating the continuous spectral density, the coordinate rotation methods[12–16] realize the function-theoretic description of a resonance as an L^2, and hence L^2-expandable, state belonging to a dilated Hamiltonian.[17–20] Still other approaches such as the J matrix[4–6,21] and certain uses of the Schwinger variational principle[22] combine a representation of the long-range part of the Hamiltonian in a complete basis with truncation of the short-range rest to a finite subject.

Most of the methods mentioned experience trouble at thresholds and when the interaction to be represented in the L^2 basis is too long-ranged. This paper deals with a prototype of such difficulty—with the dipole interaction in atomic multiphoton processes. As simple, but nontrivial, test cases of physical and recent[23–26] theoretical interest, the two-photon processes of the Bethe-logarithm[27–31] contribution to the Lamb shift and two-photon ionization near, or above the one-photon threshold in the hydrogen atom are studied. By applying and extending the discovery of Yamani and Reinhardt[9] of an L^2 discretization of the radial Coulomb Hamiltonian in a special Laguerre-Slater basis, extremely compact formulas are obtained for the double radial integrals on which the two-photon processes depend. In practice, the Laguerre-Slater basis strikes the right compromise for the efficient calculation of atomic multiphoton processes. Because the radial-integral formulas exhibit a transparent dependence on both the basis-set parameters and on the electron energy and angular momentum, it is almost straightforward, for instance, to remove the singularities explicitly that inhibit the calculation of the Bethe logarithm and to extrapolate from the information possessed by the first dozen functions to a complete-basis converged approximant of the two-photon ionization cross section. Yet, since the basis functions are linear combinations of simple Slater functions, there is no difficulty coupling the representation of the electronic continua to a traditional atomic-structure code to extend what is learned from hydrogen to other atoms.

The plan of this paper is first to satisfy the reader interested in the physical results and how the new methods introduced here compare with other recent calculations.[23–26,31] After Sec. II presents the calculation of the Bethe logarithm starting with the very compact analytical form of the ac Stark shift of arbitrarily highly excited Rydberg states afforded by the correct choice of Laguerre-Slater basis, Sec. III gives a new, computationally efficient scheme for computing the two-photon ioniza-

tion of those states, with special attention to the difficult region just around the single-photon ionization threshold. The success of the two prototype calculations, however, stems from a thorough mathematical analysis of the Laguerre-Slater basis representation of the attractive Coulomb spectrum by Pollaczek functions,[9,32,33] which is given in detail in Appendix A. The optimal form of the ac Stark shift and the current treatment of high-energy divergence in the Bethe logarithm, for example, require an extensive use of the recursion relations and asymptotic form of the Pollaczek functions, while an understanding of their various branches allows using Klarsfeld and Maquet's convergence-acceleration idea to generate a parametrization of the two-photon ionization cross section which converges rapidly and passes smoothly through the one-photon threshold. Thus, Appendix A summarizes and extends the work of Yamani *et al.*[6,9] to include the useful special cases and develop efficient, reliable algorithms to serve as the mathematical foundation of the two applications in Secs. II and III.

The final discussion in Sec. IV assesses what can be learned from the prototype calculations which is of use for many-electron atoms and large field strengths. The major lesson is the importance of careful preparation of slowly converging matrix elements in extrapolating from a modest basis set to completeness. The success of the epsilon algorithm[15,34] in analytically continuing two-photon transition amplitudes below threshold, for example, suggests a new, less empirical approach to quantum-defect theory. Moreover, the transparent dependence of the Coulomb resolvent matrix on the Slater exponent of the basis set opens a path of convergence acceleration of complex basis function[12–16] calculations. Hence, the work presented in this paper can be seen as a contribution to the effort to endow L^2-basis-set methods with extrapolation possibilities as rich and as efficient as those enjoyed by other numerical approaches.

II. BETHE-LOGARITHM-SUM CONTRIBUTION TO HYDROGENIC LAMB SHIFT

Although most of the terms of the lowest-order expansion for the Lamb shift in hydrogen can be determined analytically, the Bethe logarithm, which contains the nonrelativistic contribution to the bound electron's self-energy, must be approximated numerically. Following Bethe and Salpeter,[27] or the more careful argument of Erickson and Yennie,[29] the Bethe logarithm can be expressed either as an integral over virtual transitions from the perturbed state to all lower energy states and back, that is, as ac Stark shifts, corrected for any divergences, or, equivalently, as an expectation value of a logarithm of the nonrelativistic Hamiltonian. Since both forms require bound-state expectation values of fairly simple operator functions of the radial Coulomb Hamiltonian, they provide an ideal test of the effectiveness of the L^2-basis representation of the Coulomb spectrum introduced by Yamani and Reinhardt.[9] After briefly reviewing the form of the Bethe logarithm and its place in the lowest order of the Lamb-shift expansion, this effectiveness is demonstrated by using the basis set to express the ac Stark shift of any Rydberg state in terms of very few of the Pollaczek functions defined in Appendix A. Then, putting the detailed knowledge of the asymptotic and analytic form of those functions which is derived and summarized in Appendix A to work to smooth singularities and remove divergences, the Bethe logarithm is calculated in two ways. First, the regularized self-energy integral over the frequency-dependent Stark shifts is estimated by Gauss-Chebyshev quadrature and then the logarithmic operator form, from which the Bethe logarithm gets its name, is approximated using the Gauss-Pollaczek quadrature of the Coulomb spectrum discovered by Yamani and Reinhardt and derived for the case needed here in the appendixes. Although the logarithmic dependence of the self-energy integrand hinders the convergence with an increasing number of weights and points in both approaches, applying the epsilon convergence-acceleration algorithm[34] to a sequence of quadrature estimates finally yields accurate values for the Bethe logarithm in good agreement with those of Maquet and Klarsfeld.[30]

To lowest order, the radiative correction, or Lamb shift, of the energy of a Coulomb bound state for nuclear change Z, of principal quantum number n, orbital angular momentum l and its projection m_l, and total electronic angular momentum $j=l\pm\frac{1}{2}$, takes the form[27,29]

$$\Delta E_{n,l,j}=\frac{4\alpha^3Z^4}{3\pi n^3}\left[\left[\ln\frac{1}{(Z\alpha)^2}+\frac{11}{24}-\frac{1}{5}\right]\delta_{l0}+\ln\left[\frac{Z^2}{2K_0}\right]+\frac{3C_{lj}}{8(2l+1)}\right], \tag{1}$$

with all energies in Hartree atomic units. While the $-\frac{1}{5}$ comes from the vacuum polarization and $C_{lj}=\pm1/(j+\frac{1}{2})$, for $j=l\pm\frac{1}{2}$ from the $\alpha/2\pi$ correction to the Bohr magneton, the rest of the terms account for the self-energy of the bound electron. The nonrelativistic part of the self-energy was defined by Bethe[27] in terms of the logarithm of an average excitation energy K_0, and can be expressed as the logarithmic expectation value[29]

$$\frac{2Z^4}{n^3}\ln\left[\frac{Z^2}{2K_0}\right]=\left\langle nlm_l\left|\mathbf{p}(H_c-E_n)\ln\left[\frac{Z^2}{2\,|H_c-E_n|}\right]\mathbf{p}\right|nlm_l\right\rangle, \tag{2a}$$

where H_c is the nonrelativistic Coulomb Hamiltonian, or equivalently, as an integral[27,31]

$$\frac{2Z^4}{n^3}\ln\left[\frac{Z^2}{2K_0}\right]=\lim_{\Omega\to\infty}\left[\mathrm{P}\int_0^\Omega d\omega\,\omega\Delta_{n,l}(\omega)+\frac{Z^2\Omega}{n^2}-\frac{2Z^4\delta_{l0}}{n^3}\ln\Omega\right] \tag{2b}$$

over frequency-dependent ac Stark shifts

$$\Delta_{n,l}(\omega)=\langle nlm_l\,|\,\mathbf{p}G_c^+(E_n-\omega)\mathbf{p}\,|\,nlm_l\rangle, \tag{3}$$

where G_c^+ is the resolvent of H_c. For $l>0$, the linear counterterm, which can be included in the integral and understood as a mass-polarization correction, since $(nlm_l\,|\,p^2\,|\,nlm_l)=Z^2/n^2$,[27] is sufficient to make the self-energy finite. In s states, on the other hand, the electron comes very close to the nucleus, giving rise to the relativistic shifts of in the first set of large parentheses in Eq. (1) and requiring, in Bethe's somewhat *ad hoc* procedure, a logarithmic cutoff between these relativistic terms and the upper limit of the nonrelativistic self-energy. Although considerable effort has subsequently been spent[28,29] to clear up inconsistencies in Bethe's argument, the naive picture of the radiative correction as a sum of second-order perturbations, or virtual transitions, made finite by physically plausible counter terms, is appropriate to the atomic-physics context of this paper. For instance, while the principal part in the frequency integral in Eq. (2b), or the absolute value in the logarithm in Eq. (2a), accounts for the real part of the singularities of the integrand at actual intermediate bound states, the imaginary part would give the natural linewidths for deexcitation.[28,35] The goal of the rest of this section is, then, to show how choosing a certain L^2-basis-set expansion can give formulas so simple and general for the ac Stark shifts that the Bethe-logarithm contribution to the Lamb shift can be calculated, even for highly excited Rydberg states.

A. ac Stark shift of hydrogenic states

Computing the second-order perturbation sum $\Delta_{n,l}(\omega)$ involves integration over the four angles and the two radii. The angular integrations are performed with the standard techniques of, first, expanding the Coulomb Green's function in partial waves,

$$G_c^+(\mathbf{r},\mathbf{r}';E)=\sum_{l,m}\frac{Y_{lm}(\hat{\mathbf{r}})G_l^+(r,r';E)Y_{lm}(\hat{\mathbf{r}}')}{rr'}\,, \tag{4}$$

and then using the Wigner-Eckert theorem on the momentum as a vector operator,[36]

$$\left\langle \frac{f}{r}l'm_l'\left|p_\lambda\right|\frac{g}{r}lm_l\right\rangle =(-1)^{l'-m_l'}\begin{pmatrix} l' & 1 & l \\ -m_l' & \lambda & m_l\end{pmatrix}\left\langle\frac{f}{r}l'\left|\left|p\right|\right|\frac{g}{r}l\right\rangle\,, \tag{5}$$

to reduce the matrix element between two typical radial functions, f and g, to a radial expectation value of an effective radial momentum operator as

$$\left\langle\frac{f}{r}l'\left|\left|p\right|\right|\frac{g}{r}l\right\rangle=\int_0^\infty dr\,f(r)p^{l'l}g(r)\,, \tag{6}$$

with $p^{l+1,l}=-i\sqrt{l+1}[d/dr-(l+1)/r]$ and $p^{l,l+1}=i\sqrt{l+1}[d/dr+(l+1)/r]$. In this way,

$$\Delta_{n,l}(\omega)=-[\Delta_{n,l,l+1}(\omega)+\Delta_{n,l,l-1}(\omega)]/(2l+1)\,, \tag{7}$$

where

$$\Delta_{n,l,L}(\omega)=\int_0^\infty dr\int_0^\infty dr'\psi_n^{l*}(r)p^{lL}G_L^+(r,r';E_n-\omega)\times p^{lL}\psi_n^l(r') \tag{8}$$

contains only the radial wave function $\psi_n^l(r)$ of the state being perturbed, and radial operators, where, naturally, when $l=0$, the $l-1$ term is absent.

In a similar, but less standard fashion, the two remaining integrals can be reduced to a sum of a few terms by choosing the appropriate basis set for each radial coordinate. As described in detail in Appendix A, the matrix elements of the radial Green's function in the Laguerre-Slater basis,

$$\varphi_n^l(r;\lambda)=(\lambda r)^{l+1}e^{-\lambda r/2}L_n^{2l+1}(\lambda r)\,,$$

have the very simple form

$$G_{nn'}^{+l}(E;\lambda)=-\frac{\lambda p_{n_<}^l(x;\lambda)q_{n_>}^{+l}(E;\lambda)}{2(E+\lambda^2/8)(n+1)_{2l+1}(n'+1)_{2l+1}}\,,$$

where p_n^l and q_n^{+l} are the Pollaczek polynomials and functions and $(n)_l$ are Pochhammer symbols with $(n)_l\equiv\Gamma(n+l)/\Gamma(n)$ and $(n)_0=1$. While not difficult to calculate, the Pollaczek functions include all the spectral properties of the resolvent, with simple poles at the bound states and a branch cut along the continuum. The radial momentum operator is also represented economically in the basis as a narrow-band matrix whose only nonzero elements are

$$p_{nn}^{l,l+1}=p_{nn}^{l+1,l}=i(n+1)_{2l+3}\sqrt{l+1}/2$$

and

$$p_{n-2n}^{l+1,l}=p_{nn-2}^{l,l+1}=-i(n-1)_{2l+3}\sqrt{l+1}/2\,. \tag{9}$$

The most important simplification comes, however, by choosing the basis-set exponent λ equal to $2/n$ to coincide with the exponential decay of the radial wave function, for this makes ψ_n^l directly proportional to the basis function $\phi_{n_r}^l(r;2/n)$, where $n_r=n-l-1$ is the state's radial quantum number. Putting the basis representations of the wave function, momentum operator, and resolvent together at $E=E_n-\omega$ with $E_n=-\lambda^2/8$ then gives

$$\Delta_{n,l+l+1}=-\frac{Z^2(l+1)(q_{n_r}^{+l+1}p_{n_r}^{l+1}-2q_{n_r}^{+l+1}p_{n_r-2}^{l+1}+q_{n_r-2}^{+l+1}p_{n_r-2}^{l+1})}{4n^3\omega(n_r+1)_{2l+1}}\,,$$

$$\Delta_{n,l,l-1}=\frac{-Z^2l}{4n^3\omega(n_r+1)_{2l+1}}\{(n+l-1)^2(n+l)^2q_{n_r}^{+l-1}p_{n_r}^{l-1}-2(n^2-l^2)[(n-1)^2-l^2]q_{n_r+2}^{+l-1}p_{n_r}^{l-1}+(n-l)^2(n-l+1)^2q_{n_r+2}^{+l-1}p_{n_r+2}^{l-1}\}\,. \tag{10}$$

Further simplification follows by recurring with Eq. (A10) and employing the Wronskian of Eq. (A18) to replace the $n_r\pm2$ terms with $n_r\pm1$ and isolate the term responsible for the linear divergence to give

$$\Delta_{n,l,l+1}=-\frac{Z^2(l+1)}{\omega}\left[\frac{(q_{n_r}^{+l+1}-q_{n_r-1}^{+l+1})(p_{n_r}^{l+1}-p_{n_r-1}^{l+1})}{n(n+l+1)^2(n_r+1)_{2l+1}}-\frac{1}{n^2}\right],$$
$$\Delta_{n,l,l-1}=-\frac{Z^2l}{\omega}\left[\frac{[(n+l-1)q_{n_r}^{+l-1}-(n-l)q_{n_r+1}^{+l-1}][(n+l-1)p_{n_r}^{l-1}-(n-l)p_{n_r+1}^{l-1}]}{n(n_r+1)_{2l+1}}-\frac{1}{n^2}\right]. \tag{11}$$

Note how the sum of the two $1/n^2$ terms in Eq. (11) is of just the right form to cancel the counter term linear in Ω in Eq. (2b).

Before subtracting out the remaining logarithmic divergence, it is computationally more efficient to reexpress the Pollaczek functions of angular momentum $l\pm1$ in terms of functions of angular momentum l. This can be done using the definitions of the Pollaczek functions as hypergeometric functions in Eqs. (A8) and (A17) with some moderately tedious manipulations of ${}_2F_1$'s with contiguous parameters[32] and gives

$$\Delta_{n,l,L}(\omega)=\frac{-Z^4P_{n,l,L}Q_{n,l,L}}{2n^3\omega(n_r+1)_{2l+1}(E-E_{l_>})l_>}+\frac{Z^2l_>}{n^2\omega}, \tag{12}$$

where $l_>$ is the greater of l and L and

$$\begin{aligned}
Q_{n,l,l+1}&=(n+l+1)q_{n_r}^{+l}-(n+l)q_{n_r-1}^{+l},\\
P_{n,l,l+1}&=(n+l+1)p_{n_r}^{l}-(n+l)p_{n_r-1}^{l},\\
Q_{n,l,l-1}&=(n-l)q_{n_r}^{+l}-(n+l)q_{n_r-1}^{+l},\\
P_{n,l,l-1}&=(n-l)p_{n_r}^{l}-(n+l)p_{n_r-1}^{l}.
\end{aligned} \tag{13}$$

In Eq. (12), the factor with $E_{l_>}=-1/2l_>^2$, denoting the lowest bound state of angular momentum $l_>-1$, stems from a pole in q_n^{+l-1} at E_l for $L=l-1$ which is absent from q_n^{+l}, but is canceled by a zero in the numerator for $L=l+1$.

This compact form, which includes the formulas given by Maquet[31] for $n\le4$ as special cases, has two distinct advantages. Equipped with the algorithms for p_n^l and q_n^l given at the end of Appendix A, $\Delta_{n,l,L}$ can be calculated efficiently and accurately, while the detailed analysis of the Pollaczek functions at the beginning of Appendix A eases the study of the frequency and quantum-number dependence. Thus, the integrand of Eq. (2b) is now in simple enough form to allow numerical integration on a fine grid after explicit separation of any singular behavior.

B. The Bethe logarithm by numerical integration

To prepare the Bethe-logarithm integrand for numerical integration, the logarithmic divergence in Eq. (2b) can be studied in terms of the large-ω behavior of the Pollaczek functions appearing in Eqs. (11) or (12). Taking the limit $T\to\infty$ and $\xi\to-1$ in Eqs. (A8) and (A28) shows that $p_n^l=[(n+1)_{2l+1}/(2l+1)!][1+O(\omega^{-1})]$ and $q_n^l=-2(2l)![1+\delta_{l0}O(\omega^{-1/2})+O(\omega^{-1})]$ as ω gets large. This determines the troublesome terms in the integrand of Eq. (2b) to be

$$\omega\Delta_{n,l,L}\sim\frac{Z^2l_>}{n^2}\mp\frac{2Z^4}{(2l+1)n^3\omega}. \tag{14}$$

In addition to subtracting out the divergent high-energy terms it is of advantage to map the integration interval onto a finite interval and to smooth the poles at real intermediate bound states to be avoided in taking the principal value. Choosing the integration variable $y=T/n=(1+2n^2\omega)^{-1/2}\in[0,1]$ for $\omega\in[0,\infty)$ obviates the $\omega^{-1/2}$ integrable singularity mentioned above Eq. (14) for s states. The Bethe logarithm so transformed then takes the form

$$\ln[2Z^{-2}K_0(n,l)]=\mathrm{P}\int_0^1 dy\,F_{n,l}+\delta_{l0}\ln(n^2), \tag{15}$$

where $F_{n,l}=-(F_{n,l,l+1}+F_{n,l,l-1})/(2l+1)$, and for $L=l\pm1$

$$F_{n,l,L}=-\frac{n^2}{2Z^4}\left[\omega\Delta_{n,l,L}-\frac{Z^2l_>}{n^2}\pm\frac{2Z^4}{n^3(2l+1)(\omega-E_n)}\right]$$
$$=y^{-1}\left[\frac{P_{n,l,L}Q_{n,l,L}}{2(n_r+1)_{2l+1}(l_>^2-T^2)}\pm\frac{2}{2l+1}\right]. \tag{16}$$

From the discussion in Appendix A 2, the poles in the integrand at any intermediate bound state are hidden in the Pollaczek functions of the second kind and the residues can be extracted with the help of Eqs. (A25)–(A26). The residue of the integrand at an intermediate state of principal quantum number ν is thus

$$r_{n,l,\nu}=-(r_{n,l,\nu,l+1}+r_{n,l,\nu,l-1})/(2l+1),$$

where

$$r_{n,l,\nu,L}=\operatorname*{Res}_{y\to y_\nu}F_{n,l,L}=\frac{l_>P_{n,l,L}^2w_l(E_\nu)}{\nu(n_r+1)_{2l+1}(\nu^2-l_>^2)}. \tag{17}$$

For $L=l-1$ and $\nu=l$, the factor ν^2-l^2 is canceled by a zero of ω_l, and a limit must be taken. Before subtracting out the poles, it is useful to examine how the integrand in Eq. (15) behaves as y goes to zero. Although the integrand has already been made finite by adding the two extra terms in Eq. (16) to the Stark shift, using Eqs. (A8) and (A28) to study the $y\to0$ limit of $F_{n,l}$ exposes a $y\ln y$ dependence for $l=0$ which would hinder the convergence

of a numerical integration. This was removed along with the residues at the intermediate state poles by defining a smoothed function,

$$\tilde{F}_{n,l}=F_{n,l}-\sum_{\nu}\frac{r_{n,l,\nu}y}{(y-y_\nu)y_\nu}+8\delta_{l0}n(1-y)^{4n-1}\times\{1+2ny[\ln y+\psi(4n+2)-\psi(2)]\}\ . \quad (18)$$

Now the integral can be split in the usual way into a smooth part and an explicitly integrable singular part, giving

$$\ln[2Z^{-2}K_0(n,l)]=\int_0^1 dy\,\tilde{F}_{n,l}+\sum_{\nu}r_{n,l,\nu}[\ln(y_\nu^{-1}-1)+y_\nu^{-1}]+\delta_{l0}[2+\ln(n^2)]\ . \quad (19)$$

The third, δ_{l0}, term in Eq. (18) subtracts the constant and $y\ln y$ dependence of $F_{n,l}$ as $y\to 0$ to produce the 2 in Eq. (19).

The results for the $1s$ Bethe logarithm obtained from a Gauss-Chebyshev quadrature (weight function $[y(1-y)]^{1/2}$) for 2^N points and weights are given in the second column of Table I. Evidently, the remaining nonanalytic, logarithmic behavior of the integrand at the end points is responsible for the somewhat disappointingly slow convergence with respect to the number of quadrature abscissas. The situation is far from hopeless, however, for the integrand is a smooth function and the Chebyshev abscissas are equally spaced in the variable $\theta=2\cos^{-1}\sqrt{y}$, suggesting that convergence-acceleration techniques could work well. The remaining columns in Table I exhibit the rapid improvement ending near the single precision of the 48-bit (binary-digit) machine used by applying the epsilon algorithm[34] to the sequence of quadrature approximants in the first column. Recall that the epsilon algorithm builds a table of Padé approximants ϵ_{2k}^j with the recursion

$$\epsilon_{k+1}^j=\epsilon_{k-1}^{j+1}+1/(\epsilon_k^{j+1}-\epsilon_k^j)\ , \quad (20)$$

starting with all the ϵ_{-1}^j defined to be zero and $\{\epsilon_0^j\}$ the sequence whose convergence is to be accelerated. It is interesting that, while the quadrature approximations in Table I bound the correct value from above, the second approximants ϵ_2^j, corresponding to Aitken's algorithm,[34] approach even closer but always from below. Unfortunately, this straddling of the final value is peculiar to the $1s$ state.

TABLE I. Gauss-Chebyshev quadrature of the Bethe logarithm for the $1s$ state of hydrogen. Quadratures of the regularized self-energy using 2^j points and weights are listed as ϵ_0^j. The further columns display the Padé approximants generated by the epsilon algorithm (Ref. 34) from that sequence of quadratures.

j	ϵ_0^j (quadrature with 2^j points)	ϵ_2^j (Aitken's algorithm)
1	3.203 282 116	2.988 350 757
2	2.994 271 130	2.981 290 184
3	2.998 513 836	2.984 093 648
4	2.985 310 010	2.984 126 994
5	2.984 428 371	2.984 128 467
6	2.984 203 771	2.984 128 550
7	2.984 147 375	2.984 128 556
8	2.984 133 261	
9	2.984 129 733	

j	ϵ_4^j	ϵ_6^j	ϵ_8^j
1	2.984 068 741	2.984 128 542	2.984 128 557
2	2.984 128 359	2.984 128 557	
3	2.984 128 542	2.984 128 557	
4	2.984 128 556		
5	2.984 128 557		

Bethe-logarithm values obtained in the same way for several hydrogenic states with principal quantum number up to 25 and angular momentum up to 7 are listed in Table II and compared with other calculations. The number of significant figures reported indicates the stability of the last three epsilon-algorithm approximants, all of which include the 512-point quadrature. Although the number of intermediate states to be subtracted and very diffuse Slater exponents of the highly excited state apparently spoil the accuracy, reasonably accurate calculations even for principal quantum numbers as high as 100 should be reasonable in double precision.

The Bethe-logarithm values in Table II compare favorably with the careful computations of the lowest eight states of Maquet and Klarsfeld,[30] who isolated the logarithmic dependence of the ac Stark shift on the frequency and integrated the rest with only a 24-point quadrature. With the more compact general formula in Eq. (12) here for the integrand, it would be possible to use the $^{\pm}q_n^{-l}$ version of Eq. (A28) to subtract off both the bound-state poles and the $\ln(1-\xi^2)$ terms exactly for arbitrary states and integrate the rest with a modest number of points to high accuracy. Yet, the remaining integral with the logarithmic terms is still too complicated in the general case to be computed analytically, although using $\ln(y)$ as an integration variable in Eq. (15) would concentrate the quadrature points where they need to be. Thus the unorthodox use here of the epsilon algorithm to extract converged results from the sequence of struggles of the direct quadrature to deal with the logarithmic singularity is computationally less than optimal, but circumvents a good deal of tedious algebra while demonstrating the power of the algorithm.

C. Equivalent quadrature of the Bethe logarithm

Instead of numerically integrating for the Bethe logarithm following Eq. (2b), one could just as well use the spectral representation of the Coulomb Green's function in Eq. (3) and perform the cutoffs at large frequency explicitly to arrive at the spectral representation of Eq. (2a) given originally by Bethe.[27] Despite its innocent appear-

TABLE II. Bethe logarithms for various hydrogenic states. Where two values are listed, the upper value is this work and the lower from Ref. 30. All values lie within the error bounds of the interpolation of Ref. 46.

n	$L=0$	$L=1$	$L=2$	$L=3$	$L=4$	$L=5$	$L=6$	$L=7$
1	2.984 125 856							
	2.984 128 555 8							
2	2.811 769 90	−0.030 016 71						
	2.811 769 893 1	−0.030 016 708 6						
3	2.767 663 61	−0.383 190 2	−0.005 232 148					
	2.767 663 612 5	−0.038 190 229 4	−0.005 232 148 1					
4	2.749 811 84	−0.041 954 9	−0.006 740 939	−0.001 733 666				
	2.749 811 840 5	−0.041 954 894 6	−0.006 740 9	−0.001 733 7				
5	2.740 823 7	−0.044 034 7	−0.007 600 754	−0.002 202 169 6	−0.000 772 104 9			
	2.740 823 7	−0.044 034 7	−0.007 600 8	−0.002 202 2	−0.000 772 1			
6	2.735 664 2	−0.045 312 2	−0.008 147 20	−0.002 502 175	−0.000 962 789	−0.000 407 922		
	2.735 664 2	−0.045 312 2	−0.008 147 2	−0.002 502	−0.000 962 8	−0.000 407 9		
7	2.732 429 1	−0.046 155 19	−0.008 519 22	−0.002 709 096	−0.001 094 473	−0.000 499 702	−0.000 249 09	
	2.732 429 1	−0.046 155 2	−0.008 519 2	−0.002 790 1	−0.001 094 5	−0.000 499 7	−0.000 240 9	
8	2.730 27	−0.046 741 35	−0.008 785 05	−0.002 859 117	−0.001 190 434	−0.000 566 533	−0.000 290 426	−0.000 153 864
	2.730 267 3	−0.046 741 3	−0.008 785 0	−0.002 859 1	−0.001 190 4	−0.000 566 5	−0.000 290 4	−0.000 153 9
10	2.727 65	−0.047 482 9	−0.009 132 28	−0.003 059 092	−0.001 319 716 8	−0.000 656 884	−0.000 357 297	−0.000 205 585
15	2.724 95	−0.048 294 98	−0.009 532 18	−0.003 298 037	−0.001 478 081	−0.000 769 215	−0.000 441 01	−0.000 270 41
20	2.723 97	−0.048 609	−0.009 694 5	−0.003 399 115	−0.001 547 27	−0.000 819 505	−0.000 479 148	−0.000 300 28
25	2.723 50	−0.048 761 8	−0.009 776	−0.003 451 32	−0.001 583 82	−0.000 846 57	−0.000 499 99	−0.000 316 81

ance, however, this form of the Bethe logarithm with its sum and integral over the Coulomb spectrum is by no means straightforward to calculate accurately. Yet, knowing that truncating the basis-set expansion of the radial Coulomb Hamiltonian generates the Gauss quadrature of such spectral integrals detailed in Appendix A 2 makes it hard to resist trying the quadrature on the spectral form of the Bethe logarithm, even though the function to be integrated is not well behaved.

To this purpose, the Pollaczek polynomials and functions in the transformed ac Stark formula in Eq. (12) were put together in accordance with Eq. (A30) as Green's matrix elements, which were then approximated by an N-term truncated basis as in Eq. (A33). This truncated spectral representation can then be integrated with respect to ω to give

$$\ln[2Z^{-2}K_0(n,l)]=\frac{n(n_r+1)_{2l+1}}{4(2l+1)}\sum_{j=1}^{N}(E_j^N-E_n)\ln\left|1-\frac{E_j^n}{E_n}\right|\sum_L\frac{\psi^2_{n,l,j,L}}{(E_j^N-E_{l_>})}-\frac{r_{n,l,l,l-1}}{2(l+1)}\ln\left|\frac{E_l-E_n}{E_n}\right|+\delta_{l0}\ln(n^2)\,, \tag{21}$$

where

$$\psi_{n,l,j,l+1}=(n+l+1)\psi^N_{n_r,j}-n_r\psi^N_{n_r-1,j}\,,$$
$$\psi_{n,l,j,l-1}=(n_r+l)\psi^N_{n_r,j}-n_r\psi^N_{n_r-1,j}\,, \tag{22}$$

are the components of the momentum matrix of Eq. (9) operating on the jth eigenvector corresponding to the eigenvalue E_j^N of the $N\times N$ matrix approximation to H_l obtained by using the first N basis functions of Eq. (A2). While the last term in Eq. (21) accounts separately and exactly for the $l-1$ bound state at E_l, the sum over pseudostates omits the exactly represented state to be perturbed trivially and approximately omits the apparent pole at E_{l+1} by a vanishing of that term in Eq. (22).

Because the other pseudostate poles cannot mimic the effect of intermediate states exactly enough and the logarithmic integrand is not well represented by a polynomial, this quadrature approach does not converge as nearly as well. Table III illustrates the equivalent quadrature estimates and their epsilon-algorithm approximates for the $1s$ Bethe logarithm. Note, for example, how the ϵ_4^3 approximant obtains three-figure accuracy from the 8-, 16-, and 32-point quadratures and that the whole epsilon tableau gives a reliable picture of the convergence behavior. Since an equivalent quadrature calculation requires only the eigenvalues and eigenvectors of the Hamiltonian in a finite L^2 basis, this moderate success suggests its use on systems where more accurate representations of the spectrum are too difficult to obtain.

TABLE III. Pollaczek equivalent quadrature of hydrogen $1s$ Bethe logarithm. Quadratures of the spectral representation of the Bethe logarithm using 2^j points and weights generated by diagonalization of the Coulomb Hamiltonian in a basis of 2^j Slater-Laguerre functions are listed as ϵ_0^j. The further columns display the Padé approximants obtained by the epsilon algorithm (Ref. 34) from that sequence of quadratures.

j	ϵ_0^j	ϵ_2^j	ϵ_4^j	ϵ_6^j
3	1.4319	3.2642	2.9818	2.9843
4	2.0023	3.0643	2.9842	
5	2.3952	3.0106	2.9843	
6	2.6427	2.9937		
7	2.7906	2.9878		
8	2.8762			
9	2.9247			

III. TWO-PHOTON IONIZATION OF HYDROGEN

The compact form in Eq. (10) of the ac Stark shift of arbitrary hydrogenic states achieved by the basis-set expansion suggests trying the same approach on the more demanding and more interesting two-photon matrix elements which give the transition amplitude for two-photon ionization. The demanding aspect appears when the absorption of the first photon produces a continuum intermediate state which then absorbs an additional photon, for then none of the functions in the second integration in the matrix element decay and the integral converges only through the destructive interference of two waves of different frequency. When the photon is somewhat redder and the intermediate slightly bound, the situation is in a certain sense even worse, for the intermediate wave function dies very slowly while the amplitude varies wildly with the frequency. Recently, Aymar and Crance[23] dealt with the intermediate continuum directly by integrating the long-range form of the intermediate wave function iteratively by parts to generate an accurate asymptotic expansion. Maquet and Klarsfeld,[26] on the other hand, extended their Sturmian-expansion representation of the intermediate Green's function from bound intermediate energies, where it converges, above the one-photon threshold to free intermediate energies, where it does not, but where the epsilon algorithm applied to the partial sums approximates the appropriate analytic continuation accurately enough, except for some difficulty just above the threshold.

This section presents a new approach to calculating multiphoton transition elements, which proves to be competitive with those of Aymar and Crance and of Maquet and Klarsfeld with the advantage of using a basis much more closely related to the functions common to atomic-structure calculations. After first reminding the reader of the dependence of the differential photoionization cross section on a few basic radial integrals, those radial integrals are expressed in the basis set as formal infinite sums containing products of Pollaczek functions. Although at light frequencies where the intermediate state is free, these sums converge no better than the corresponding radial integrals with their oscillating integrands, the results of the detailed analysis of the asymptotic properties of the various branches of the Pollaczek functions in Appendix A can be exploited to split the formal sums into

geometric-series-like components on which the epsilon algorithm works very well. In addition, the division of the intermediate Pollaczek function at slightly bound energies into a background and a resonant part leads to a very efficient parametrization of the widely varying transition amplitudes by smoothly varying functions.

A. Reduction of cross sections to radial integrals

In the lowest order in the dipole interaction of light of frequency ω with an atom, the differential cross section for two-photon ionization can be defined as[23,36]

$$d\sigma_2/d\Omega=\pi\omega\,|\,T_{f0}\,|^2 7.3170\times10^{-43}\ \mathrm{m^4\,W^{-1}}\ , \tag{23}$$

where, for hydrogen

$$T_{f0}=\langle E_f,\hat{\mathbf{k}}_f\,|\,\mathrm{dip}\,G^+(E_i)\mathrm{dip}\,|\,nlm_l\rangle \tag{24}$$

is the transition amplitude from a bound state (n,l,m_l) of energy E_n, dipole coupled (dip) to an intermediate state of energy $E_i=E_n+\omega$, to a final photoelectron of energy $E_f=E_i+\omega$, in direction $\hat{\mathbf{k}}_f$. The numerical factor in Eq. (23) converts from Hartree atomic to SI units.

Assuming, as is usually the case in experiments, that the initial bound state is a statistical mixture of angular momentum projections, but that the light has polarization λ, with $\lambda=\pm1$ for circularly polarized light propagating along the laboratory **z** direction or $\lambda=0$ for linearized polarized light propagating along the **x** direction, leads to an expansion of the differential photoionization cross section in the first three even Legendre polynomials ($L=0,2,4$):

$$d\sigma_2(n,l,\omega,\lambda)/d\Omega=\sum_L P_L(\cos\theta)d_L(n,l,\omega,\lambda)/4\pi \tag{25}$$

with[36]

$$d_L(n,l,\omega,\lambda)=\frac{\pi\omega(2L+1)(-1)^l}{4(2l+1)}\sum_{l_f}\sum_{l_f'}\sum_{l_i}\sum_{l_i'}(2l_f'+1)^{1/2}(2l_f+1)^{1/2}\begin{bmatrix}l_f' & l_f & L\\ 0 & 0 & 0\end{bmatrix}$$
$$\times\begin{bmatrix}L_i' & L_i & L\\ -2 & 2 & 0\end{bmatrix}\begin{Bmatrix}L_i' & L_i & L\\ l_f & l_f' & l\end{Bmatrix}(2L_i+1)\begin{bmatrix}1 & 1 & L_i\\ \lambda & \lambda & -2\lambda\end{bmatrix}$$
$$\times\tau^{l_fL_il}(n,\omega)(2L_i'+1)\begin{bmatrix}1 & 1 & L_i'\\ \lambda & \lambda & -2\lambda\end{bmatrix}[\tau^{l_f'L_i'l}(n,\omega)]^*\ , \tag{26}$$

where

$$\tau^{l_fL_il}(n,\omega)=\sum_{l_i}\begin{Bmatrix}l & 1 & l_i\\ 1 & l_f & L_i\end{Bmatrix}t^{l_fl_il}(n,\omega) \tag{27}$$

are recouplings of the radial transition matrix elements, in the notation of Eq. (6),

$$t^{l_fl_il}(n,\omega)=-\omega^{-2}\langle E_fl_f\,|\,p^{l_fl_i}G_{l_i}^+(E_i)p^{l_il}\,|\,nl\rangle\ . \tag{28}$$

For the s initial-state calculations presented below, the form of the three expansion coefficients d_L simplifies greatly, for the intermediate must be a p state—giving only one term in the sum in Eq. (27) with $L_i=l_f$. Indeed, for circularly polarized light, this allows only d photoelectrons and lets the cross section be written most simply as

$$d\sigma_2^{\mathrm{circ}}/d\Omega(n,s,\omega)=\omega\,|\,t^{dps}(n,\omega)\,|^2\sin^4\theta/128\ , \tag{29}$$

now in Hartree atomic units, without the numerical factor of Eq. (23).

With linearly polarized light, on the other hand, both s and d photoelectrons are emitted and the Legendre polynomial expansion is still the most useful:

$$d_0^{\mathrm{lin}}(n,s,\omega)=\sigma_2^{\mathrm{lin}}=\pi\omega(\,|\,t^{sps}\,|^2/36+\,|\,t^{dps}\,|^2/90)\ ,$$
$$d_2^{\mathrm{lin}}(n,s,\omega)=\pi\omega[\,|\,t^{dps}\,|^2/63-\mathrm{Re}(t^{sps}t^{*dps})/9\sqrt{2}]\ , \tag{30}$$
$$d_4^{\mathrm{lin}}(n,s,\omega)=\pi\omega\,|\,t^{dps}\,|^2/35\ .$$

Note that the only information on the relative phase of proceeding to the two possible final angular momenta is contained in the angular dependence of the differential cross section, in d_2.

B. Calculation of the radial integrals

After this introduction on the dependence of the photoionization cross section on a few radial transition matrix elements, a new, efficient way of calculating them using the same basis set as for the shift can be presented. Just as for the ac Stark shift in Sec. II A, the Laguerre-Slater basis of Eq. (A2) generates the narrow-band matrix of Eq. (9) for the radial momentum, the resolvent matrix of Eq. (A30), and, for the special choice of the exponent, $\lambda=2/n$, includes the initial state exactly as the member of the basis, $\phi_{n_r}^l(r;2/n)$, where $n_r\equiv n-l-1$ is the radial quantum number. Then, expanding the final continuum radial wave function in accordance with Eq. (A5) gives the formal sum for the transition element,

$$t^{l_fl_il}(n,\omega)$$
$$=-\frac{[\psi_0^{+l_f}(E_f)]^*(2l_f+1)!}{\omega^2 n}$$
$$\times\sum_{n_f}\sum_{n_i}\sum_{n_i'}\frac{p_{n_f}^{l_f}(x_f)p_{n_fn_i}^{l_fl_i}G_{n_in_i'}^{+l_i}(E_i)p_{n_i'n_r}^{l_il}}{(n_f+1)_{2l_f+1}[(n_r+1)_{2l+1}]^{1/2}}\ , \tag{31}$$

where $x_f=(E_f+E_n)/(E_f-E_n)$ in accordance with Eq.

(A8) and the $\lambda=2/n$ dependence of $p_n^{l_f}$ and $G_{nn'}^{+l_i}$ is suppressed. Since, by Eq. (9), the momentum matrices $p_{n'n}^{l_i l}$ vanish unless $n'=n$ or $n\pm2$, only a single infinite sum remains in Eq. (31). To avoid needlessly lengthy formulas, a discussion of the particular case $(l_f,l_i,l)=(d,p,s)$ suffices to illustrate the method. Evaluating the momentum matrix for this case then displays the single infinite sum as

$$t^{dps}(n,\omega)=\frac{30\sqrt{2}[\psi_0^{+d}(E_f)]^*}{n^{1/2}\omega^2}\sum_{j=0}^{\infty}(p_j^d-p_{j-2}^d)[\,G_{jn_r}^{+p}(n+2)(n+1)-G_{j,n_r-2}^{+p}(n-2)(n-1)]\,, \tag{32}$$

where any terms with negative indices here, and in the expressions to follow, are defined to be zero. When going further to introduce the greater and/or lesser product in Eq. (A30) for the resolvent matrix, it is expedient to use the Wronskian of Eq. (A18) to reach the compact form

$$t^{dps}(n,\omega)=-\frac{30\sqrt{2}[\psi_0^{+d}(E_f)]^*}{n^{5/2}\omega^3}\left[\sum_{j=0}^{n_r-1}\frac{(p_j^d-p_{j-2}^d)}{(j+1)_3}p_j^p(q_{n_r}^{+p}-q_{n_r-2}^{+p})+\sum_{j=n_r}^{\infty}\frac{(p_j^d-p_{j-2}^d)}{(n+1)_3}q_j^{+p}(p_{n_r}^p-p_{n_r-2}^p)\right.$$
$$\left.-\frac{2(p_{n_r-1}^d-p_{n_r-3}^d)}{n+1}\right], \tag{33}$$

with $x_i=(E_i+E_n)/(E_i-E_n)$. The last term corrects for the cases in the sums where the greater and/or lesser rule is violated.

Looking at Eq. (33) and knowing from Appendix A that the Pollaczek polynomials and functions are easily calculated, one might ask why the work is not now over. The trouble comes when the intermediate energy E_i is not significantly negative, as must be expected from the oscillatory transition element being approximated in the exponentially decaying basis functions; the infinite sum in Eq. (33) does not converge. From Eqs. (A17a) and (A27a), for positive E_i, the product $p_j^d q_j^{+p}=O(j^3)$ for large j, whence the terms in the infinite sum acquire constant amplitude with increasing j, albeit with a wildly enough oscillating phase to ensure convergence in some appropriate sense. That the partial sums show no sign of convergence occurred also in Klarsfeld and Maquet's Sturmian expansion,[26] and their experience suggests that the epsilon convergence-acceleration algorithm so useful in improving the quadrature estimates of the Lamb shift in Sec. II can save this otherwise dismal situation. Now, the sort of sums where the epsilon algorithm works best are geometriclike series in a complex variable z, at or even outside the radius of convergence, for the algorithm generates a Padé approximant in z to the analytic continuation of the formal series. Here, this geometriclike behavior can be mimicked for positive E by using Eq. (A24) to split $p_j^d(x_f)$ into $[q_j^{+d}(E_f)-q_j^{-d}(E_f)]/2\pi i\rho_d(E_f)$ so that for large j, the summands are dominated in accordance with Eq. (A17a) by the asymptotic behavior $(\xi_f\xi_i)^{j+1}$ for the q_j^{+d} sum and (ξ_i/ξ_f) for the q_j^{-d} sum, with ξ_i and ξ_f the appropriate energy-dependent complex numbers of unit modulus defined below Eq. (A8). Table IV displays the epsilon-algorithm approximants to the two parts obtained by splitting the infinite sum in Eq. (33) for the ionization of the $1s$ state with a frequency large enough to proceed through a slightly unbound intermediate state and using only the

TABLE IV. Convergence acceleration above the one-photon threshold. The first row gives the partial sums up to 15 terms of the two parts of the basis-set expansion of the two-photon ionization of the $1s$ state of atomic hydrogen with circularly polarized light of frequency 0.51 a.u., as discussed below Eq. (33) in the text. The further rows display the Padé approximants, $[14-k/k]$ generated by the epsilon algorithm (Ref. 34) from the sequence of partial sums of 15 and fewer terms.

Iteration	Approximants to	
k	$\sum_{n=0}^{\infty}(q_n^{+d}-q_{n-2}^{+d})q_n^{+p}/(n+1)_3$	$\sum_{n=0}^{\infty}(q_n^{-d}-q_{n-2}^{-d})q_n^{+p}/(n+1)_3$
0	$-36.585\,594\,72-1.313\,247\,628i$	$178.632\,027\,6-172.885\,722\,9i$
1	$-68.908\,805\,73-69.964\,399\,43i$	$47.985\,140\,67-197.207\,182\,5i$
2	$-69.290\,317\,38-70.137\,098\,55i$	$49.202\,043\,92-197.583\,533\,9i$
3	$-69.295\,932\,01-70.136\,203\,10i$	$49.173\,688\,78-197.573\,879\,6i$
4	$-69.296\,052\,70-70.136\,116\,89i$	$49.174\,934\,31-197.573\,773\,0i$
5	$-69.296\,056\,58-70.136\,111\,24i$	$49.174\,946\,35-197.573\,675\,5i$
6	$-69.296\,056\,77-70.136\,110\,72i$	$49.174\,869\,37-197.573\,811\,8i$

TABLE V. (a) Two-photon ionization of *ns* states of atomic hydrogen above the one-photon threshold by circularly polarized light. Sources were a, this work; b, Aymar and Crance (Ref. 23); c, Klarsfeld and Maquet (Ref. 26). Cross sections in cm/W, where (−44) indicates a factor of 10^{-44}. (b) Cross section for ionization by linearly polarized light (this work). (c) Asymmetry parameter d_2 for linearly polarized light.

λ/n	Source	$n=1$	$n=2$	$n=3$	$n=4$	$n=5$	$n=6$
				(a)			
20	a	1.10(−44)	8.8(−42)	4.2(−40)			
	b	1.10(−44)					
	c	1.11(−44)					
100	a	3.02(−40)	2.105(−37)	9.23(−36)	1.30(−34)	9.78(−34)	4.92(−34)
	b	3.02(−40)	2.10(−37)	9.24(−36)	1.30(−34)	9.78(−34)	4.93(−34)
	c	2.99(−40)	2.09(−37)	9.20(−36)	1.30(−34)	9.75(−34)	4.91(−34)
300	a	3.219(−37)	1.957(−34)	7.485(−33)	9.13(−32)	6.02(−31)	2.71(−30)
	b	3.22(−37)	1.96(−34)	7.39(−33)	9.15(−32)	6.02(−31)	2.71(−30)
	c	3.33(−37)	1.95(−34)	7.46(−33)	9.10(−32)	6.00(−31)	2.70(−30)
400	a	2.028(−36)	1.154(−33)	4.134(−32)	4.784(−31)	3.032(−30)	1.33(−29)
	b	2.03(−36)	1.15(−33)	4.14(−32)	4.79(−31)	3.03(−30)	1.33(−29)
	c	2.02(−37)	1.15(−33)	4.12(−32)	4.77(−31)	3.02(−30)	1.33(−29)
500	a	8.534(−36)	4.530(−33)	1.572(−31)	1.692(−30)	1.042(−29)	4.49(−29)
	b	8.54(−36)	4.53(−33)	1.53(−31)	1.69(−30)	1.04(−29)	4.50(−29)
	c	8.52(−36)	4.50(−33)	1.52(−31)	1.69(−30)	1.04(−29)	4.4(−29)
600	a	2.786(−35)	1.374(−32)	4.378(−31)	4.680(−30)	2.821(−29)	1.201(−28)
	b	2.79(−35)	1.37(−32)	4.38(−31)	4.68(−30)	2.82(−29)	1.20(−28)
	c	2.77(−35)	1.38(−32)	4.37(−31)	4.66(−30)	2.81(−29)	1.2(−28)
700	a	7.639(−35)	3.486(−32)	1.055(−30)	1.094(−29)	6.486(−29)	2.74(−28)
	b	7.64(−35)	3.49(−32)	1.06(−30)	1.09(−29)	6.49(−29)	2.74(−28)
	c	7.64(−35)	3.46(−32)	1.05(−30)	1.09(−29)	6.4(−29)	
800	a	1.846(−34)	7.765(−32)	2.239(−30)	2.264(−29)	1.325(−28)	5.55(−28)
	b	1.85(−34)	7.77(−32)	2.24(−30)	2.27(−29)	1.33(−28)	5.56(−28)
	c	1.85(−34)		2.23(−30)	2.3(−29)		
900	a	4.057(−34)	1.566(−31)	4.317(−30)	4.272(−29)	2.474(−28)	1.032(−27)
	b	4.06(−34)	1.57(−31)	4.32(−30)	4.30(−29)	2.48(−29)	1.03(−27)
911.27	a	4.412(−34)	1.686(−31)	4.625(−30)	4.567(−29)	2.642(−28)	1.10(−27)
	b	4.41(−34)	1.69(−31)	4.63(−30)	4.57(−29)	2.65(−29)	1.10(−27)
				(b)			
20		1.61(−44)	1.27(−41)	5.7(−40)			
100		4.090(−40)	2.605(−37)	1.05(−35)	1.38(−34)	9.9(−34)	4.9(−33)
300		3.668(−37)	1.991(−34)	7.144(−33)	8.48(−32)	5.53(−31)	2.49(−30)
400		2.151(−36)	1.107(−33)	3.795(−32)	4.33(−31)	2.75(−30)	1.22(−29)
500		8.493(−36)	4.156(−33)	1.364(−31)	1.508(−30)	9.37(−30)	4.09(−29)
600		2.619(−35)	1.216(−32)	3.830(−31)	4.125(−30)	2.52(−29)	1.09(−28)
700		6.826(−35)	2.997(−32)	9.080(−31)	9.564(−30)	5.784(−29)	2.49(−28)
800		1.577(−34)	6.516(−32)	1.903(−30)	1.967(−29)	1.179(−28)	5.06(−28)
900		3.332(−34)	1.287(−31)	3.630(−30)	3.694(−29)	2.199(−28)	9.41(−28)
911.27		3.608(−34)	1.383(−31)	3.885(−30)	3.947(−29)	2.348(−28)	1.00(−27)
				(c)			
20		4.32(−44)	2.75(−41)				
100		8.31(−40)	9.84(−38)	−8.20(−36)	−1.67(−34)	−1.15(−33)	−4.3(−33)
300		2.814(−37)	−2.014(−34)	−6.811(−33)	−3.13(−32)	1.22(−30)	1.77(−30)
400		6.761(−37)	−1.168(−33)	−2.276(−32)	4.50(−32)	1.91(−30)	1.39(−29)
500		−2.400(−37)	−3.887(−33)	−3.261(−32)	7.458(−31)	9.85(−30)	5.96(−29)
600		−7.045(−36)	−8.939(−33)	3.671(−32)	3.372(−30)	3.36(−29)	1.85(−28)
700		−2.847(−35)	−1.489(−32)	3.615(−31)	1.040(−29)	9.02(−29)	4.69(−28)
800		−7.610(−34)	−1.588(−32)	1.273(−30)	2.590(−29)	2.059(−28)	1.03(−27)
900		−1.583(−33)	1.456(−33)	3.309(−30)	5.593(−29)	4.187(−28)	2.04(−27)
911.27		−1.697(−33)	5.50(−33)	3.641(−30)	6.058(−29)	4.51(−27)	2.19(−27)

first 15 partial sums. Evidently, the lion's share of the convergence acceleration is accomplished in the first step, where Aitken's algorithm generates a single pole in the variables, $(\xi_i\xi_f)$ or (ξ_i/ξ_f) in the approximation. To be honest, at the low values of E_i and numbers of terms used in the approximant, the discussion of the low-energy asymptotics of the Pollaczek functions in Appendix A reveals that the series are not all that geometric and the epsilon algorithm is performing more subtly to achieve such impressive convergence acceleration. Table V exhibits the cross-section parameters for a variety of initial s states at several frequencies and compares with the previous results of Aymar and Crance, and Klarsfeld and Maquet.

When the intermediate energy is negative, on the other hand, q_j^{+p} dies eventually exponentially as ξ_i^{j+1} as j becomes large and one might hope that the infinite sum for the transition element in Eq. (33) converges rapidly enough. Yet, the analysis in Appendix A exposes the practical fallacy of this supposition, for the exponential decay only sets in when $j+l_i+1\approx T_i^3/4n$, which is much too late when the intermediate is only slightly bound and hence T_i large. To make matters worse, the Airy-function-like dependence of $q_j^{+p}(E_i)$ on j and its rich Rydberg pole structure at slightly negative E_i make the infinite sum a poor candidate for successful convergence acceleration. The rather surprising solution to this dilemma is to reexpress the too-slowly-convergent infinite sum with two formally divergent, but geometriclike sums, and then let the epsilon algorithm go to work.

Using Eq. (A26) to split $q_j^{+p}(E_i)$ into its two other neighboring branches ${}^{\pm}q_j^{-p}$, and defining

$$\mathscr{E}^{\pm}=\sum_{j=n_r}^{\infty}[q_j^{+d}(E_f)-q_{j-2}^{+d}(E_f)]^{\pm}q_j^{-p}(E_i)/(j+1)_3\ , \quad (34)$$

gives two formally divergent sums whose analytic continuation is efficiently approximated by the epsilon algorithm applied to the sequence of partial sums. Table VI demonstrates a rate of convergence again for the 1s ionization, but with E_i just bound, which is every bit as good as for positive E_i. Since $q_j^{+p}(E_i)$ at negative E_i is real, the necessary sums with $q_j^{-d}(E)$ can be obtained from Eq. (34) by appropriate combination of $\mathscr{E}^+$ and $\mathscr{E}^-$.

The tremendous advantage of employing the other branches, ${}^{\pm}q_j^{-p}$, comes not from the improved convergence alone, but rather from the additional possibility of an unambiguous, smooth splitting of the transition element into a background and a resonant part:

$$t^{l_f l_i l}(n,\omega)=t_{\rm back}^{l_f l_i l}(n,\omega)-t_{\rm res}^{l_f l_i l}(n,\omega)\cot(\pi T_i)\ , \quad (35)$$

where $T_i=(-2E_i)^{-1/2}$, with poles at each intermediate bound Coulomb state at T_i-l_i a positive integer. Incorporating the definition of $\mathscr{E}^{\pm}$ of Eq. (34) and the relation between the branches of q_n^p of Eq. (A26) into Eq. (33) for the transition element gives

$$t_{\rm back}^{dps}=-\frac{30\sqrt{2}(\psi_0^{+d})^*}{(n)^{5/2}\omega^3}\left[\sum_{j=0}^{n_r-1}\frac{(p_j^d-p_{j-2}^d)p_j^p}{(j+1)_3}\mathrm{Re}({}^{+}q_{n_r}^{-p}-{}^{+}q_{n_r-2}^{-p})+\frac{\mathrm{Im}(\mathscr{E}^{+}+\mathscr{E}^{-})}{2\pi\rho_d}(p_{n_r}^p-p_{n_r-2}^p)\right.$$

$$\left.-2(p_{n_r-1}^d-p_{n_r-3}^d)/(n+1)\right]\ , \quad (36)$$

$$t_{\rm res}^{dps}=-\frac{30\sqrt{2}(\psi_0^{+d})^*}{n^{5/2}\omega^3}\left[\sum_{j=0}^{n_r-1}\frac{(p_j^d-p_{j-2}^d)p_j^p}{(j+1)_3}\mathrm{Im}({}^{+}q_{n_r}^{-p}-{}^{+}q_{n_r-2}^{-p})+\frac{\mathrm{Re}(\mathscr{E}^{+}-\mathscr{E}^{-})}{2\pi\rho_d}(p_{n_r}^p-p_{n_r-2}^p)\right]\ . \quad (37)$$

TABLE VI. Convergence acceleration below the one-photon threshold. The first row gives the partial sums up to 15 terms of the two formally divergent parts discussed below Eq. (34) in the text for the transition amplitude for the two-photon ionization of the 1s state of atomic hydrogen with circularly polarized light of frequency 0.49 a.u. The further rows display the Padé approximants, $[14-k/k]$, generated by the epsilon algorithm (Ref. 34) from the sequence of partial sums of 15 and fewer terms.

Iteration	Approximants to	
k	$\sum_{n=0}^{\infty}(q_n^{+d}-q_{n-2}^{+d})^{+}q_n^{-p}/(n+1)_3$	$\sum_{n=0}^{\infty}(q_n^{+d}-q_{n-2}^{+d})^{-}q_n^{-p}/(n+1)_3$
0	131.224 895 5+318.309 173 4i	−33.576 456 19−155.171 204 3i
1	48.869 503 58+196.292 811 9i	−74.926 665 55−66.997 079 24i
2	49.272 645 29+198.036 167 4i	−74.892 268 80−66.228 458 04i
3	49.263 748 68+197.984 914 4i	−74.886 049 94−66.215 705 94i
4	49.264 915 83+197.987 280 8i	−74.885 714 71−66.215 371 04i
5	49.264 728 08+197.987 127 0i	−74.885 691 90−66.215 357 69i
6	49.264 760 70+197.987 161 5i	−74.885 689 65−66.215 356 88i

Since, for $E_i<0$, the expressions in brackets are real, it is now easy to extract the phase of the remaining complex quantity ψ_0^{+d} to define the real quantity

$$\tilde{t}^{l_f l_i l}(n,\omega)=(e^{i\sigma_{l_f}})(\pi n^5\omega^7)^{1/2}t^{l_f l_i l}(n,\omega)\ , \tag{38}$$

where $\sigma_{l_f}=\arg\Gamma(l_f+1-T_f)$ is the Coulomb phase shift of the final continuum partial wave and the additional factors scale away much of the energy and initial-quantum-number dependence.[26] The total scaled transition element $\tilde{t}$ is plotted for the $1s$ initial state and d or s final partial waves in Figs. 1 and 2, respectively. Above the one-photon threshold, where E_i becomes positive, the graphs switch to display the real and imaginary parts and the absolute value of the now complex scaled transition element $\tilde{t}$. Examination of Eqs. (A27a) and (A27b) reveals that the smooth transition from $\tilde{t}_{\rm back}$ below threshold to the real part of $\tilde{t}$ above threshold and from $\tilde{t}_{\rm res}$ to the imaginary part of $\tilde{t}$ is no accident.

The kink in Fig. 1, at a frequency of about 0.46 hartree just below the resonance at the $n=4$ intermediate p state, indicates the numerical limitations of the present extrapolation procedure. At such strongly bound intermediate energies, the minus branch form of Eq. (A28) requires a large number of terms and great care to avoid cancellation errors. Moreover, the infinite sum in Eq. (A28) can only be efficiently performed at large n, and, near a Rydberg-state energy, the relation for recurring to smaller n becomes ill conditioned. The larger the initial principal quantum number and the more negative the intermediate energy, the more severe this problem becomes, as can be seen from Figs. 3 and 4. There, the scaled transition elements for Eq. (38) for the transition from each of the first five s states through p to s continua performed with $n+10$ basis functions are plotted against the frequency stretched by n^2 to make the curves easier to compare. Below $n^2\omega$ about 0.45, the extrapolation of especially the background part of $\tilde{t}$ becomes more and more erratic with increasing n, indicating a numerical inability of the epsilon algorithm to continue the formally divergent $\tilde{t}_{\rm back}$ to $\tilde{t}_{\rm res}$ down that far in energy. The same calculation performed with a few more basis functions gives graphical agreement with Figs. 3 and 4, down to about $n^2\omega=0.45$, where erratic disagreement takes over. Although work is in progress to remove this limitation, it does not present a serious hindrance to the calculation of two-photon transition amplitudes, for, just at strongly bound intermediates, the straightforward approach using the plus branch of Pollaczek functions in Eq. (33) works well. Hence the best algorithm for the present uses Eq. (33) when E_i is sufficiently negative and switches over to computing the formally divergent, but geometriclike series only when E_i

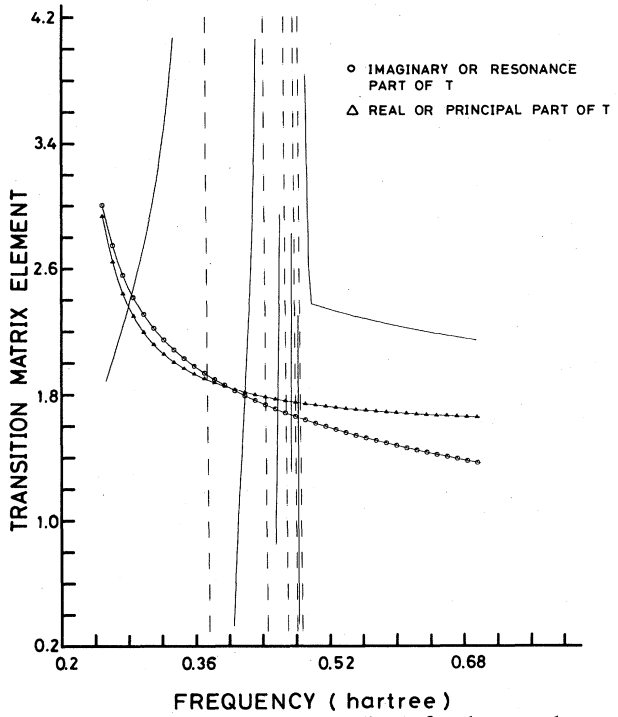

FIG. 1. Scaled radial transition amplitude for the two-photon ionization of the hydrogen $1s$ state through a p intermediate to an s continuum. Above the one-photon ionization threshold at $\omega=0.5$ hartree, the amplitude is smooth and complex; the absolute value in atomic units is indicated by the simple solid line, its real part by the line marked with triangles and the imaginary part by circles. Below $\omega=0.5$, the amplitude becomes real with poles at each intermediate Rydberg state, the first few of which are denoted by the dashed vertical asymptotes. It can be smoothly parametrized by $\tilde{t}=\tilde{t}_{\rm back}-\tilde{t}_{\rm res}/\tan\pi T$ where $\tilde{t}_{\rm back}$ and $\tilde{t}_{\rm res}$ are the smooth continuations of the real and imaginary parts below the one-photon threshold. Calculated using ten basis functions.

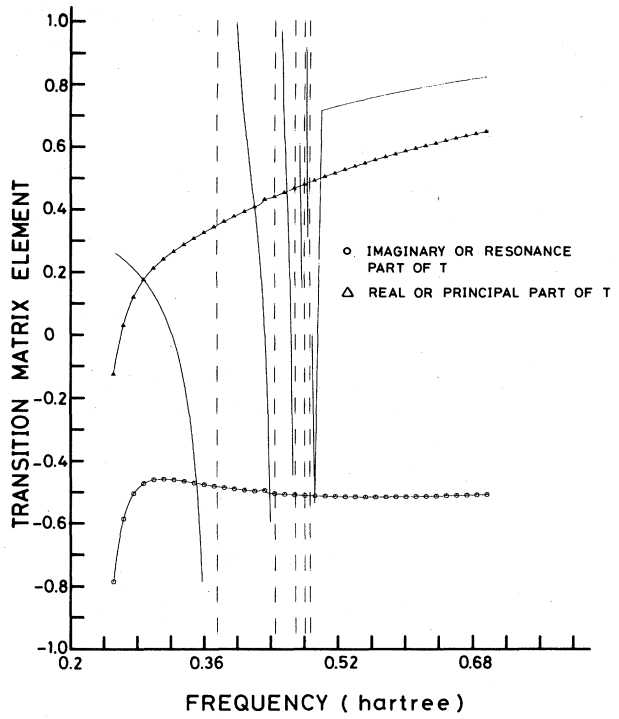

FIG. 2. Scaled radial transition amplitude for the two-photon ionization of the hydrogen $1s$ state through a p intermediate to a d continuum. Absolute value, real or background, and imaginary or resonance parts as in Fig. 1.

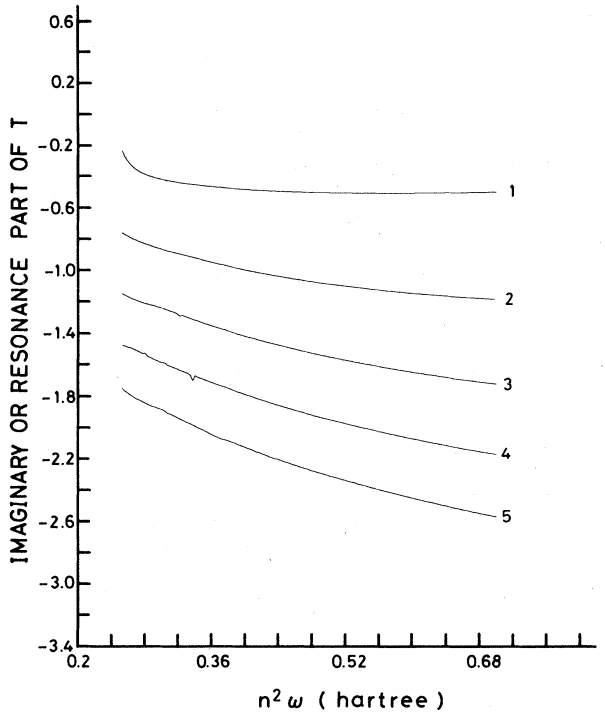

FIG. 3. Imaginary or resonance part of the scaled radial transition element in atomic units for two-photon ionization of the first five s states of hydrogen through a p intermediate to an s continuum vs the frequency stretched by the principle quantum number squared. Calculated using $n+10$ basis functions. Note that the threshold for one-photon ionization is at $n^2\omega=0.5$ hartree and that the values depicted are reliable only above $n^2\omega\approx 0.45$.

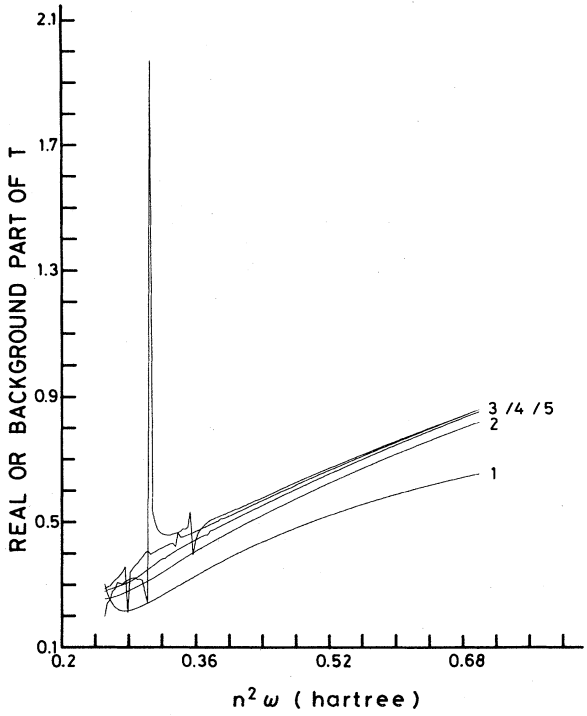

FIG. 4. Real or background part of the scaled radial transition element in atomic units for two-photon ionization of the first five s states of hydrogen through a p intermediate to an s continuum vs the frequency stretched by the principle quantum number squared. Note that the threshold for one-photon ionization is at $n^2\omega=0.5$ hartree and that the wild oscillations indicate that the values are reliable only above $n^2\omega=0.45$.

is slightly negative—say at the onset of the exponential decay of q_j^+ with j at $T_i^3\approx 2nN_i$, where N_i is the number of basis functions.

In a general sense, the two-photon ionization cross-section calculations of Aymar and Crance, Maquet, and this work have much in common. While Aymar and Crance integrate the appropriate inhomogeneous differential equation out to a radius where the integrand over the remainder achieves its asymptotic behavior and repeated integration by parts of the remainder generates a rapidly converging sequence, Maquet and this work, following his suggestion, sum a basis-set expansion up to an index j, where the epsilon algorithm can perform the analogous task in function space. The splitting of the radial transition amplitudes into matrix elements with two Jost solutions, in close analogy to Aymar and Crance's iteration with the sum and difference of WKB phases, has the double advantage of solving the problem the Sturmian basis has in correctly representing the multivalued structure of the amplitude at the one-photon threshold and of providing a well-defined separation into background and resonant contributions just below that threshold. Indeed, this preparation of poorly converging partial sums containing a polynomial with sinelike asymptotic form into two sums containing functions with complex-exponential behavior may prove valuable in other instances such as the summation of partial-wave expansions. Perhaps the strongest point in favor of the basis set of Eq. (A2) is not revealed by the hydrogen-atom applications presented here, however, and that is the ease with which such a basis set can be coupled to a traditional Slater-type basis function atomic-structure code. While supplementing such a structure code with 10—15 additional functions shown to be sufficient in this work for each ionized radial degree of freedom is no small change, still the well-developed technology of representing bound states by basis functions can be exploited optimally.

IV. DISCUSSION

Now that the test of the L^2-basis-set approach for calculating slowly converging matrix elements came out surprisingly well, it is fitting to explore extending the method to obtain reliable atomic multiphoton transition amplitudes. Of importance are how the basis can represent a many-electron atom with an ionization continuum and Rydberg series, how the epsilon algorithm estimates complete-basis results, what must be changed to exploit the advantages of dilation analytically[17–20] by using complex basis functions, and how to treat the Rydberg states in strong fields.

The Laguerre-Slater basis of Eq. (2) seems to strike the right compromise between aptness for bound states and for continua needed in calculating photoionization pro-

cesses. While exponentially decaying basis functions can represent the initial bound state as well as the residual ionic core economically, the solubility of the radial Coulomb equation in the special basis affords a correct treatment of the analytic structure of the resolvent operator, with its many branches and accumulating poles. Particularly promising appears the introduction of the smoothly varying branches, ${}^{\pm}q_n^-$, at negative energies, in analogy to Seaton's formulation of quantum-defect theory.[38] Since various branches of the resolvent matrix differ by separable terms, the scattering and transition operators and the Fredholm determinant in a multichannel problem can be separated formally into background and resonance contributions. This immediately allows a basis-set calculation of quantum defects by searching for the zeros of the Fredholm determinant obtained either by the J-matrix method[5] or, better, by a Schwinger variational approach.[22]

The epsilon algorithm proved here to be both versatile and powerful. While its efficiency at extrapolating the Chebyshev quadratures of the Bethe logarithm is to be expected, its ability to approximate the complete-basis limit in the equivalent-quadrature Bethe logarithm and two-photon ionization calculations is astounding. The well-converged approximants below the one-photon threshold in Table VI define, at least numerically, an analytic continuation of formally divergent transition elements from a bound state to an exploding wave. This corresponds to continuing Aymar and Crance's[23] partial integration approach below threshold by discarding divergent surface terms and suggests a new way of defining and computing quantum defects as negative-energy phase shifts, not only at the bound states, but in between. Yet, the approach seems only to work well when the matrix elements to be extrapolated are split into sequences with some similarity to a geometric series, even if formally divergent. Perhaps the splitting merely serves to define the branch of the function to be extrapolated uniquely. Further study of how the epsilon algorithm analytically continues is important; it could suggest efficient ways to treat such problems as three-body scattering and breakup with basis-set approaches.

The close relation of the basis set of Eq. (A2) to the Slater type has another ramification of current interest in contributing to the understanding of complex-dilation approaches which employ complex Slater exponents.[12–16] Since the dependence of the Pollaczek polynomials and functions is transparent from their hypergeometric representations, it is directly clear how the spectrum and resolvent react to complex scaling. Whereas the independence of $\Gamma(l+1-T)$ in Eqs. (A5) and (A17) indicates immediately the invariance of the discrete spectrum, the conformal map form of the λ dependence of ξ and x exposes the rotation of the branch cut between ingoing and outgoing waves, or between q_n^+ and q_n^-, down into the complex energy plane. Two consequences of making λ complex show promise when examined in light of the experience gained with basis-set convergence acceleration here. First, although Eq. (A6) for the regular wave function becomes even more of a formal, indeed divergent, series, the epsilon algorithm should be able to continue its exploding part analytically. Second, the diagonal dominance of the resolvent matrix in Eq. (A30) achieved by choosing a negative argument for λ at real energies, because then $|\xi|$ is less than 1, provides hope that partial ionization probabilities for quite complicated processes may be projected out of entirely L^2 complex basis representations by convergence-acceleration techniques applied at the end of the calculation.[15]

Simply turning up the electromagnetic field strength to a measurable fraction of the atomic field also generates an atom-plus-field system too complex to be solved straightforwardly, even for the hydrogen atom. The nonperturbative Floquet truncated complex-basis-function calculations of Chu and Reinhardt[12] give insight into the intricacies of a correct treatment of the time development of the atomic states in a strong optical frequency field. Unfortunately, their truncated basis does not represent the accumulation of dressed Rydberg states at the threshold for a free-free transition. The recent experiments of Kruit *et al.*[39] revealed a surprising disappearance without appreciable shift of the lowest-energy photoelectron peak, which provoked Tip and Muller's[40] careful analysis of the role of the A^2 term in shifting the effective threshold. Work is in progress in this laboratory to incorporate the compact and smooth representation of the Coulomb threshold developed here into a nonperturbative description of atomic multiphoton ionization involving highly excited Rydberg intermediate states.

ACKNOWLEDGMENTS

The author acknowledges stimulating discussions with and the helpful advice of Dr. Peter Pfeifer, Dr. Friedrich Biegler-König, and Professor Jürgen Hinze, and the support of the Universität Bielefeld and the Deutsche Forschungsgemeinschaft (Sonderforschungsbereich 216, "Polarization and Correlation in Atomic Collision Complexes").

APPENDIX A: BASIS-SET REPRESENTATION OF THE COULOMB SPECTRUM

Several years ago, Yamani and Reinhardt[9] discovered that the Schrödinger equation for the radial Coulomb Hamiltonian for angular momentum l and nuclear charge Z,

$$H_l = -\tfrac{1}{2}d^2/dr^2 + l(l+1)/2r^2 - Z/r \ , \tag{A1}$$

in the complete basis,

$$\varphi_n^l(r;\lambda) = (\lambda r)^{l+1} e^{-\lambda r/2} L_n^{2l+1}(\lambda r), \quad n = 0,1,\ldots \tag{A2}$$

can be solved analytically giving expansion coefficients for the regular wave function and the resolvent of H_l in terms of certain hypergeometric functions which had been investigated by Pollaczek.[32,33] With Appendix B, this appendix summarizes and extends their results to give a direct proof of the orthogonality of the Pollaczek polynomials, to elucidate the Gauss quadrature of the Coulomb spectral density associated with them, and to investigate the properties of the Pollaczek functions thoroughly

enough to afford stable algorithms for their rapid and accurate numerical calculation.

The basis set in Eq. (A2) is orthogonal on $[0,\infty)$ with respect to the metric $1/r$ so that

$$\int_0^\infty dr\,\varphi_n^l(r;\lambda)r^{-1}\varphi_{n'}^l(r;\lambda)=\delta_{nn'}(n+1)_{2l+1}\,, \tag{A3}$$

where $(a)_b=\Gamma(a+b)/\Gamma(a)$ is the Pochhammer symbol.[32] This means that the overlap matrix $S_{nn'}=\int_0^\infty dr\,\phi_n^l\phi_{n'}^l$ is not diagonal, but rather tridiagonal, with nonzero matrix elements:

$$\begin{aligned}S_{nn}&=2(n+l+1)(n+1)_{2l+1}/\lambda\,,\\ S_{n,n+1}&=S_{n+1,n}=-(n+1)_{2l+2}/\lambda\,.\end{aligned}$$

Moreover, the matrix of the radial Coulomb Hamiltonian in Eq. (A1) in the basis is also of symmetric tridiagonal, or Jacobi, form with nonzero elements:

$$\begin{aligned}H_{nn}&=\lambda^2S_{nn}/8-Z(n+1)_{2l+1}\,,\\ H_{n,n+1}&=H_{n+1,n}=-\lambda^2S_{n,n+1}/8\,.\end{aligned} \tag{A4}$$

With such a simple form for the Hamilton matrix, it is not surprising that eigenfunction expansion coefficients and the elements of the resolvent matrix can be expressed in terms of analytically known functions. For the regular solution,[41]

$$\psi_l^+(r;E)=\frac{e^{\pi t/2}\Gamma(l+1-T)}{\sqrt{2\pi k}\,(2l+1)!}(2kr)^{l+1}e^{ikr}\times\Phi(l+1-T,2l+2;-2ikr)\,, \tag{A5}$$

where $E=k^2/2$, $t=Z/k$, and $T=it$, the formal expansion

$$\psi_l^+(r;E)=\sum_{n=0}^\infty\varphi_n^l(r;\lambda)\psi_n^{+l}(E;\lambda) \tag{A6}$$

has coefficients

$$\psi_n^{+l}(E;\lambda)=\psi_0^{+l}(E;\lambda)p_n^l(x;\lambda)\Big/\begin{bmatrix}n+2l+1\\2l+1\end{bmatrix} \tag{A7}$$

containing Pollaczek polynomials[9,32,33]

$$\begin{aligned}p_n^l(x;\lambda)&=P_n^{l+1}(x;-\tau,\tau)\\&=\begin{bmatrix}n+2l+1\\2l+1\end{bmatrix}(-\xi)^n\times{}_2F_1(-n,l+1-T;2l+2;1-\xi^{-2})\,,\end{aligned} \tag{A8}$$

where $\tau=2Z/\lambda$, $\xi=(T-\tau)/(T+\tau)=\exp(i\zeta)$, $x=(E-\lambda^2/8)/(E+\lambda^2/8)=-\cos\zeta$, and the initial value in n,

$$\psi_0^{+l}(E;\lambda)=\frac{e^{\pi t/2}\Gamma(l+1-T)}{\sqrt{2\pi k}\,(2l+1)!}(2\sin\zeta)^{l+1}\xi^T\,. \tag{A9}$$

Indeed, the Pollaczek polynomials here are only a renormalization of the Sturm-sequence polynomials in x for the Jacobi matrix $(H_l-ES)/(E+\lambda^2/8)$; they obey the three-term recursion

$$(n+1)p_{n+1}^l-2[(n+l+1-\tau)x+\tau]p_n^l+(n+2l+1)p_{n-1}^l=0\,, \tag{A10}$$

with initial conditions: $p_0^l\equiv1$, $p_{-1}^l\equiv0$. Thus, except for the interesting special case when $\tau-l$ is a positive integer, discussed below, the p_n^l are polynomials of degree n in x. As shown explicitly in Appendix B, they are orthogonal with respect to the weight function,

$$\rho_l(x)=e^{\pi t}\xi^{2T}(2\sin\zeta)^{2l+1}\times\Gamma(l+1-T)\Gamma(l+1+T)/\pi\,, \tag{A11}$$

giving

$$\oint\!\!\!\!\!\!\int d\rho_l(x)p_n^lp_{n'}^l=\delta_{nn'}(n+1)_{2l+1}/(n+l+1-\tau)\,. \tag{A12}$$

Here, $\oint\!\!\!\!\!\!\int d\rho_l$ symbolizes a Stieltjes sort of integral, with an integral for $x\in[-1,1]$, corresponding to positive energies, and an infinite sum of jumps of $-2\pi i\,\mathrm{Res}(\rho_l)$ at the poles of $\Gamma(l+1-T)$, which lie at real x values to the right and left of the integration region, corresponding to the Rydberg series. The evident connection between the completeness of the solutions to the Schrödinger equation and the orthogonality is detailed in Appendix B.

When, as is useful in the applications in Secs. II and III, the exponent λ in the basis is chosen so that $\tau-l$ is a positive integer, the orthogonality integral in Eq. (A12) would blow up at one n, and the above discussion must be modified. When $\tau=2Z/\lambda=n_r+l+1$, where $n_r\geq0$, the basis function $\phi_{n_r}^l(r,\lambda)$ is a constant times the Coulomb bound eigenstate of energy $E=-\lambda^2/8$, and is hence superfluous in the expansion of the continuum eigenstate $\psi_l^+(r,E)$. A look at the recursion relation (A10) in this case reveals that the p_n^l are polynomials of degree $n-1$, and not n, in x for $n>n_r$. One could say that one of the zeros of each of these polynomials has been pushed to $x\to\infty$, which corresponds exactly to $E=-\lambda^2/8$. The simplest way out of this dilemma is, then, to remove $p_{n_r}^l$ from the set of polynomials as well as the residue in the Stieltjes-type integral as $x\to\infty$. This reduced set of polynomials fulfill the appropriately modified recursion and orthogonality relations.

1. Pollaczek equivalent quadrature

As recognized by Heller *et al.*,[10] the orthogonality of the polynomials leads directly to a Gauss quadrature especially tailored to approximate integrals over the Coulomb spectral density of the form

$$\langle i\mid O(H_l)\mid f\rangle=\oint\!\!\!\!\!\!\int dE\langle i\mid\psi_l^+(E)\rangle O(E)\langle\psi_l^+(E)\mid f\rangle\,, \tag{A13}$$

where O is some operator function of H_l. Using the basis-set expansion in Eq. (A6) truncated to the first N terms and performing at the same time a Gauss quadrature with abscissas at the zeros of the Nth Pollaczek polynomial leads to the very simple approximation,

$$\langle i \mid O(H_l) \mid f \rangle \approx \sum_{j=1}^{N} \langle i \mid \psi_j^N \rangle O(E_j^N) \langle \psi_j^N \mid f \rangle \ , \quad \text{(A14)}$$

where

$$\psi_j^N(r) = \sum_{n=0}^{N-1} \varphi_n^l(r) \psi_{nj}^N \quad \text{(A15)}$$

is the jth normalized eigenvector of H_l truncated to an $N \times N$ matrix. The expansion coefficients are then the Sturm-sequence polynomials scaled by the quadrature weights w_j^N,

$$\psi_{nj}^N = [2(E+\lambda^2/8) w_j^N/\lambda]^{1/2} \times (n!) p_n^l(x_j^N;\lambda)/(n+2l+1)! \ . \quad \text{(A16)}$$

If the basis-set exponent is chosen so that one of the N basis functions corresponds to an exact Coulomb bound state, the argument must be modified to treat that state separately and exactly and approximate the rest of the spectrum by the remaining $N-1$ pseudostates. At the end, the exact state takes its place among the pseudostates again as one of the terms in the sum in Eq. (A14).

2. Pollaczek functions of the second kind

Since the basis-set representation of the Schrödinger equation, Eq. (A10), is a three-term recursion relation, it is quite analogous to a second-order differential equation. Hence, in addition to the regular solution, p_n^l, expressing the resolvent matrix requires a second, linearly independent solution with Weyl or Jost behavior,[5,19] irregular in n at $n=0$ and dying exponentially at large n in the positive half momentum plane and oscillatory in the $E+i\epsilon$ limit. The function with this behavior is[4,5]

$$q_n^{+l}(E;\lambda) = \frac{-2(n+2l+1)!(-\xi)^{n+1}\Gamma(l+1-T)}{\Gamma(n+l+2-T)} \times {}_2F_1(-l-T, n+1; n+l+2-T; \xi^2) \ , \quad \text{(A17)}$$

and because it is one of the set of Kummer's hypergeometric functions[32] having the same parameters as the Pollaczek polynomial, q_n^{+l} should by all rights be called a Pollaczek function of the second kind. The recursion for this second solution differs only from that of p_n^l in the initial condition $q_{-1}^l = -2[(2l)!]$, which gives the very simple discrete analogy to the Wronskian:

$$W(q^+, p) := (q_n^{+l} p_{n-1}^l - q_{n-1}^{+l} p_n^l)/2(n+1)_{2l} = 1 \ , \quad \text{(A18)}$$

independent of n.

Following the same approach used to prove the orthogonality of the Pollaczek polynomials in Appendix B, it is straightforward to establish the integral representation,

$$q_n^{+l}(x) = \oint\!\!\!\!\!\!- \, d\rho_l(x') p_n^l(x')/(x'-x) \ , \quad \text{(A19)}$$

except for an extra term in q_0^l for the special choice of Slater exponent, $\tau = l+1$, corresponding to an exact representation of the lowest bound state of angular momentum l. Although this representation of the second function as a Stieltjes-type integral is not useful for actual computation, it immediately suggests two calculational approaches.

First, by adding and subtracting p_n^l to the integrand in Eq. (A19), the singularity in the integrand can be separated into a smooth part and a simple singular part,

$$q_n^{+l}(E;\lambda) = \bar{q}_n^l(x;\lambda) + p_n^l(x;\lambda) q_0^{+l}(E;\lambda) \ , \quad \text{(A20)}$$

in such a way that the smooth part can be expressed exactly with the help of the quadrature discussed in Appendix A 1 as

$$\bar{q}_n^l(x;\lambda) = p_n^l(x;\lambda) {\sum_{j=1}^{n}}' w_j^n/(x_j^n - x) \ , \quad \text{(A21)}$$

where the primed sum indicates omission of the exactly represented bound state if $\tau - l$ is a positive integer. Because p_0^l is chosen equal to 1, the $\bar{q}_n^l$ obey the recursion relation (A10) with the initial conditions $\bar{q}_0^l = 0$ and $\bar{q}_{-1}^l = -2(2l)!$. Moreover, Eq. (A21) with Eq. (A20) can be used to write q_0^{+l} as the Gauss quadrature approximation of its integral representation plus an error term:

$$q_0^{+l}(E;\lambda) = {\sum_{j=1}^{n}}' w_j^n/(x_j^n - x) + q_n^{+l}(E;\lambda)/p_n^l(x;\lambda) \ . \quad \text{(A22)}$$

For $|\xi| < 1$ in Eq. (A18) and away from the bound-state poles at $T-l$ equal to positive integers, the error term dies exponentially with increasing n, making the quadrature approximation even better. This can be achieved as well at positive energies simply by choosing a complex Slater exponent λ, with $\mathrm{Im}\lambda < 0$, thus indicating explicitly how well complex-dilated finite-basis calculations can be expected to work. Evidently, from the definition of ξ below Eq. (A8), the error term will be much larger near threshold, where $|k/\lambda|$ is small, and at large $|k/\lambda|$ than at intermediate energies.

Second, the integral representation in Eq. (19) exposes the many-valued nature of the Pollaczek functions of the second kind. Replacing k by $-k$, and hence T by $-T$ and ξ by ξ^{-1} in Eq. (A17) gives another branch:

$$q_n^{-l}(E;\lambda) = \frac{-2(n+2l+1)!(-\xi)^{-n-1}\Gamma(l+1+T)}{\Gamma(n+l+2+T)} \times {}_2F_1(-l+T, n+1; n+l+2+T; \xi^{-2}) \ , \quad \text{(A23)}$$

where the hypergeometric series converges for $|\xi| > 1$, or $\mathrm{Im}(k/\lambda) < 0$. The appropriate Kummer's relation[32] expresses this solution as a linear combination of the other two:

$$q_n^{-l}(E;\lambda) = q_n^{+l} - 2\pi i \rho_l p_n^l \ . \quad \text{(A24)}$$

In the limit towards real positive energies, Eqs. (A17) and (A23) are complex conjugates of each other, and the second term in Eq. (A24) displays the discontinuity across the scattering branch cut in terms of the spectral density and the expansion coefficient of the regular Coulomb wave. Yet, a good look at Eqs. (A5), (A9), or (A11) reveals that this square-root cut structure in the Pollaczek

function of the second kind is not the whole story; the Coulomb potential introduces a logarithmic manifold of Riemann sheets through the term, $\exp(\pi t/2)$. Indeed, when k is positive imaginary, and hence T positive real, two useful branches appear from two ways of forming $(-1)^T$. Then it is expedient to replace the weight function ρ_l, which is complex at such negative energy, by

$$w_l=(\xi^2)^T(\xi-\xi^{-1})^{2l+1}\Gamma(l+1-T)/\Gamma(-l-T)\ , \qquad \text{(A25)}$$

which is real at both negative and positive energies assuming real λ, with $\rho_l=iw_l\exp(-i\pi T)/\sin(\pi T)$. The two branches can then be chosen as

$$\begin{aligned}{}^{\pm}q_n^{-l}&=q_n^{+l}+\frac{2\pi e^{\mp i\pi T}}{\sin(\pi T)}w_l p_n^l\\&=q_n^{+l}+\frac{2\pi}{\tan(\pi T)}w_l p_n^l\mp 2\pi i w_l p_n^l\ ,\end{aligned} \qquad \text{(A26)}$$

so that they are complex conjugates of one another for positive imaginary k, this time with discontinuity $2\pi i w_l p_n^l$. Moreover, it follows from the formulas for ρ_l, w_l, and q_n^{+l} in Eqs. (A11), (A25), and (A17) that the factor $2\pi w_l p_n^l\cot(\pi T)$ in Eq. (A26) just cancels the bound-state pole in q_n^{+l} to give functions which are smooth in the upper half k plane. Although the existence of two branches in Eq. (A26) indicates that the hypergeometric series for q_n^{-l} in Eq. (A23) is a divergent, formal sum,

$$\begin{aligned}q_n^{+l}=2w_l\Bigg[&-p_n^l[\pi\cot(\pi T)+\ln(\xi^{-2}-1)]\\&+\begin{bmatrix}n+2l+1\\2l+1\end{bmatrix}(-\xi)^n\Bigg[\sum_{\nu=-2l-1}^{-1}\frac{(-n)_\nu(l+1-T)_\nu\Gamma(-\nu)(1-\xi^{-2})^\nu}{(2l+2)_\nu}\\&+\sum_{\nu=0}^{n}\frac{(-n)_\nu(l+1-T)_\nu h_\nu(1-\xi^{-2})^\nu}{(2l+2)_\nu(\nu!)}\\&-\frac{2(l+1-T)_{n+1}(\xi-\xi^{-1})^{n+1}}{\xi(n+1)!(n+2l+2)}\\&\times{}_3F_2(n+l+2-T,1,1;n+2l+3,n+2;1-\xi^{-2})\Bigg]\Bigg]\ ,\end{aligned} \qquad \text{(A28)}$$

where

$$\begin{aligned}h_\nu:=\ &\psi(\nu+2l+2)+\psi(\nu+1)-\psi(n+1-\nu)\\&-\psi(-l-\nu+T)\ ,\end{aligned}$$

which is not simply a sum of ${}_2F_1$'s but has the logarithmic term because two of the parameters of the hypergeometric function in Eq. (A17) differ by an integer. When $|\xi^{-2}-1|$ is less than 1, Eq. (A28) gives not only a convergent sum for q_n^{+l}, but also for the other branches ${}^{\pm}q_n^{+l}$, through Eqs. (A23) and (A26) and, at real E and λ for their real part, $\tilde{q}_n^l$. The expression for q_n^{-l} corresponding to Eq. (A28) but with $-T$ and ξ^{-1} in place of T and ξ converges for $|1-\xi^2|<1$ to give an alternative direct route to q_n^l sometimes useful at negative energies.

${}^{+}q_n^{-l}$ goes over into q_n^{-l} as the energy becomes positive on the physical sheet, where the series for q_n^{+l} converges, while ${}^{-}q_n^{-l}$ acquires an additional factor of $\exp(-2\pi t)$.

Now we can collect the reward for this rather lengthy discourse on the analytic structure of the Pollaczek functions by identifying functions, ${}^{\pm}q_n^{-l}$, which remain smooth when passing from positive to negative energies, much in the spirit of the quantum-defect idea.[38] Denoting the real part of ${}^{\pm}q_n^{-}$ in Eq. (A26) by $\tilde{q}_n^l$ affords the splitting

$$q_n^{+l}=\tilde{q}_n^l+i\pi\rho_l p_n^l \qquad \text{(A27a)}$$

for E real positive so that $\tilde{q}_n^l$ is the principle value of the integral in Eq. (A19) when k and λ are real positive, and

$$q_n^{+l}=\tilde{q}_n^l-2\pi w_l p_n^l\cot(\pi T) \qquad \text{(A27b)}$$

for E real negative, which separates q_n^{+l} into a background contribution $\tilde{q}_n^l$, and a resonance contribution with poles at each bound state when $T-l$ is a positive integer. This splitting proves essential to the numerical stability of the calculation of two-photon ionization amplitudes in Sec. III. Although for moderately negative energies the hypergeometric series converges best for q_n^{+l} directly and not for ${}^{\pm}q_n^{-}$, for very small or large energies, when ξ^2 is close to 1, it is of advantage to use the analytic continuation

3. The resolvent matrix

Now, equipped with the two linearly independent solutions satisfying the appropriate boundary conditions, it is easy to obtain the coefficient matrix in the formal basis set expansion of the resolvent of H_l,[6,21,41]

$$G_l^+(r,r';E)=\sum_n\sum_{n'}\varphi_n^l(r;\lambda)G_{nn'}^{+l}(E;\lambda)\varphi_{n'}^l(r';\lambda)\ , \qquad \text{(A29)}$$

as

$$G_{nn'}^{+l}(E;\lambda)=\frac{-\lambda p_{n_<}^l(x;\lambda)q_{n_>}^{+l}(E;\lambda)}{2(E+\lambda^2/8)(n+1)_{2l+1}(n'+1)_{2l+1}}\ , \qquad \text{(A30)}$$

where $n_<$ and $n_>$ are the lesser and greater of n and n', as might be expected from the close analogy between the

three-term recursion (A10) and a second-order differential equation. At the special, energy-dependent, Sturmiam[31,42] choice of Slater exponent, $\lambda=\sqrt{-8E}$, where $\tau=T$ and $\xi=0$, the matrix collapses to the diagonal form $G^{+l}_{nn'}=\delta_{nn'}T/[(n+1)_{2l+1}(T-n-l-1)]$.

Following an argument similar to that in Appendix B leading to the orthogonality of the Pollaczek polynomials establishes the integral representation:

$$G^l_{nn'}=\frac{\lambda}{2(E+\lambda^2/8)}\oint'\frac{d\rho_l(x')p^l_n(x')p^l_{n'}(x')}{(x-x')(n+1)_{2l+1}(n'+1)_{2l+1}}+\frac{\delta_{nn_r}\delta_{n_rn'}}{(E+\lambda^2/8)S_{n_rn_r}}\ . \tag{A31}$$

The last term appears only if $T-l=n_r+1$ is a positive integer and gives the normalized contribution of the one exactly represented bound state of radial quantum number, n_r. Subtracting and adding the residue in the integrand at $x'=x$ so regularizes part of the integral to allow an exact Gauss quadrature of degree $N>n$,

$$G^{+l}_{nn'}=\bar{G}^{\,l}_{nn'}(E;\lambda)-\frac{\lambda q^{+l}_N p^l_n p^l_{n'}}{2(E+\lambda^2/8)p^l_N(n+1)_{2l+1}(n'+1)_{2l+1}}\ , \tag{A32}$$

where, following the notation in Appendix A 2,

$$\bar{G}^{\,l}_{nn'}=\sum_{j=1}^{N}\psi^N_{nj}\psi^N_{n'j}/(E-E_j)\ , \tag{A33}$$

which includes the exactly represented bound state and the pseudostates.

Clearly, the quadrature approximation is good when $n_>$ is sufficiently smaller than N and $|\xi|<1$. Just as for the approximation for q^{+l}_0 in Eq. (A22), choosing $\mathrm{Im}\lambda<0$ decreases $|\xi|$, improving the quadrature representation by rotating the pseudostate eigenvalues away from the real positive energy axis, but only helps significantly at intermediate energies.

Finally, other branches of the resolvent matrix are expressed with the other branches of the Pollaczek function in Eq. (A30), where Eq. (A26) also leads to the background and resonant splitting at negative energies.

4. Large-n behavior of the Pollaczek functions

The success of employing, and especially accelerating the convergence of, such basis-set expansions as Eq. (A6) for the wave function and Eq. (A29) for the Green's function hinge on a thorough understanding of the asymptotic behavior of the Pollaczek polynomials and functions. Clearly, neither of the formal sums converges in n uniformly in r, or for that matter in E. To mimic the actual oscillatory wave function at larger and larger r, more and more of the exponentially decaying basis functions are required. The only hope is that the description of the physical process of interest involves either a matrix element with a short-ranged operator or an exponentially dying function or that the large-n behavior is smooth and reveals itself at low enough n to allow accurate extrapolation.

The very-large-n behavior is exposed by a Kummer's transformation[32] of Eq. (A17):

$$q^{+l}_n(E;\lambda)=\frac{-2(n+2l+1)!(-\xi)^{n+1}(1-\xi^2)^{l+T}}{(l+1-T)_{n+1}}{}_2F_1(-l-T,l+1-T;n+l+2-T;(1-\xi^{-2})^{-1})\ . \tag{A17'}$$

Denoting $n+l+1$ by m and using the Stirling formula for gamma functions and the ${}_2F_1$ in Eq. (A17') as an asymptotic series gives

$$q^{+l}_n(E;\lambda)=-2\Gamma(l+1-T)(-\xi)^{m-l}\times[m(1-\xi^2)]^{l+T}[1+O(m^{-1})]\ \text{ as } m\to\infty\ ,$$

but this is only the dominant behavior for $m\gg T$ and $m+1\gg(-l-T)(l+1-T)(1-\xi^{-2})^{-1}$. At least this reveals the Weyl's solution behavior of q^{+l}_n,[5,19] decreasing eventually exponentially with ξ^n for $|\xi|<1$ and oscillating indefinitely when $|\xi|=1$.

On the other hand, the asymptotic behavior is of little use near threshold. In the extreme case, when $|T|\to\infty$ at fixed n, it is not hard to see that the simultaneous limits $\xi^2\to1$ and $T\to\infty$ cause the hypergeometric series in Eqs. (A8) and (A17) to flow together into the confluent hypergeometric functions[32]

$$p^l_n(x;\lambda)\sim(-1)^nL^{2l+1}_n(4\tau)\ \text{ as } T\to\infty\ ,$$

$$q^{+l}_n(x;\lambda)\sim-2(n+2l+1)!(-1)^n(4\tau)^{2l+1}\times\psi(n+2l+2;2l+2;-4\tau+i0)\ .$$

The more complicated expansion in Eq. (A28) is considerably more useful in this respect, however, for the only infinite sum there, the ${}_3F_2$, has two gamma functions in the denominator to ensure a useful asymptotic expansion in n even when the large value of T in the numerator multiplies with the argument to give a finite limit and eventually an ${}_2F_2$.

Approximating the three-term recursion relation in Eq. (A10) as a difference equation[43] in the continuous variable, $m=n+l+1$, gives a second-order differential equation in m whose asymptotic behavior can be unified by a WKB approach. The study shows q^{+l}_n to act as an Airy function with increasing m, switching from real oscillatory to exponentially decaying when $m\approx T^2/\tau$, which can only occur at negative E. At positive E, on the other hand, q^{+l}_n remains complex oscillatory, but with amplitude smooth in n. The final ξ^{n+l} behavior sets in late, when $m\approx T^3/4\tau$. The $^{\pm}q^{-l}_n$, in contrast, act as other branches of the Airy function, with smooth-amplitude complex oscillations at all real energies. Naturally, the p^l_n exhibit the typical polynominal behavior, with oscillations in the region of the pseudostate eigenvalues and exponentially increasing in absolute value at higher and lower en-

ergies. The conclusions to be drawn are that the p_n^l are not so suitable for extrapolation techniques, the q_n^{+l} suitable only when T is not large real positive (just below threshold) and the ${}^{\pm}q_n^{-l}$ at all real energies.

5. Stable algorithms for the Pollaczek functions

Because the three-term recursion (A10) involves so few arithmetic operations, the temptation to use it directly to generate the desired set of q and p is hard to resist. Yet, especially with diffuse Slater exponents, and hence large τ, needed to represent highly excited Rydberg states, the coefficient of p_n^l in Eq. (A10) becomes large, magnifying roundoff errors disastrously in each step. A simple remedy is to recur instead for the ratio of two neighboring functions and then multiply out later. In fact, this scheme is very efficient and stable enough to use for the Pollaczek polynomials and, letting $r_n^l = p_n^l / p_{n-1}^l$, runs as follows.

Initialize: $1/r_0^l := 0$, $p_0^l := 1$.
Recur from $n=0$ to $N-1$:

$$r_{n+1}^l = [\,(2n+2l+2)x + 2\tau(1-x) - (n+2l+1)/r_n^l\,]/(n+1)\,. \tag{A34}$$

Then $p_{n+1}^l = r_{n+1}^l p_n^l$.

It turns out that even for large l, where the second term might be expected to magnify the error, the ratio r_n^l grows fast enough to ensure stability.

The situation is quite different for the Pollaczek functions of the second kind, however. Examining the large-n behavior of q_n^{+l} given below Eq. (A17a) reveals scheme (A34) to be unstable for $|\xi| < 1$, and especially so at negative energies. Here, a recursion downward damps roundoff errors, as might be expected from the nature of the q_n^{+l} as Weyl solutions fulfilling a boundary condition at large n.[5,19] At intermediate energies, the Gauss continued fraction[32,44] directly for $r_n^l = q_n^{+l}/q_{n-1}^{+l}$ provides an extremely efficient initialization. When ξ^2 is too close to 1 for the continued fraction to converge well, the logarithmic expansion in Eq. (A28) can be used, where the ${}_3F_2$ sum converges best at the highest n values needed to start a downward recursion. The error estimates given by Luke[41] for a special case of the Gauss fraction help in choosing which of the two initial values should be computed, to give the following algorithm.

Initialize: $r_N^{+l} = q_N^{+l}/q_{N-1}^{+l}$ from Gauss fraction or Eq. (A28).
Recur down from $n=N-1$ to 0:

$$r_n^l = (n+2l+1)/[2n+2l+2+2\tau(1-x) - (n+1)r_{n+1}^l]\,. \tag{A35}$$

Initialize: $q_{-1}^l = -2[(2l)!]$.
Recur up from $n=0$ to N: $q_n^{+l} = r_n^{+l} q_{n-1}^{+l}$.

The other branches, ${}^{\pm}q_n^{-l}$, as well as $\tilde{q}_n^l$ can be obtained once q_n^{+l} and p_n^l are known, or especially at energies near the bound-state poles, directly from the upward recursion (A34) initialized with q_0^{-l} from the Gauss fraction. If very accurate values are required, for example to test the stability of recursions (A34) and (A35), it is always possible to compute precise values for the first and last functions and to solve the recursion as a system of linear equations with iterative improvement.[45] This has the advantage of explicitly displaying the recursion error, but is considerably less efficient. Although the careful attention to numerical stability leading to Eqs. (A34) for p_n^l and (A35) for q_n^{+l} proved to be essential in the applications presented in Secs. II and III, this last refinement was only needed as a check.

APPENDIX B: ORTHOGONALITY OF THE POLLACZEK POLYNOMIALS

The orthogonality of the Pollaczek polynomials was demonstrated by Szegö[46] soon after their introduction using a generating function approach but with the parameters limited to correspond here to the repulsive Coulomb case, thus avoiding the sum over bound states. Although the extension of that method to include the attractive Coulomb spectrum is straightforward, it is more constructive for the physical understanding to make explicit use of the Pollaczek functions. The proof starts by reexpressing the orthogonality integral over the continuous spectrum in terms of a closed contour integral containing a product of a Pollaczek function with a Pollaczek polynomial, which is evaluated as a sum of residues at each bound state and at one additional pole present only when the two polynomials are equal.

To that effect, examine

$$I_{nn'}^l(\lambda) = \int_{-1}^{1} dx\, \rho_l(x;\lambda) p_n^l(x;\lambda) p_{n'}^l(x;\lambda)\,. \tag{B1}$$

Without loss of generality, assume $n \geq n'$ and express $\rho_l p_n^l$ using Eq. (A24) in terms of q_n^{+l} and q_n^{-l}. Then change the variable of integration to $\xi = (T-\tau)/(T+\tau)$ from Eq. (A8), transforming the path of integration, assuming $\tau = 2/\lambda$ is real positive, into the upper unit semicircle in the complex ξ plane. An inspection of Eq. (A23) and Eq. (A17) reveals that q_n^{-l} on this upper unit semicircle is just q_n^{+l} on the lower unit semicircle, giving

$$I_{nn'}^l = (4\pi i)^{-1} \oint d\xi (\xi^{-2}-1) q_n^{+l} p_{n'}^l\,, \tag{B2}$$

where the integrand is well behaved on the integration path. To compute the residues at the poles inside the unit circle contour, start with the bound-state singularities in Eq. (A17) for q_n^{+l} where $T-l-1 = n_b - l - 1$, positive integer or zero. The corresponding ξ_b lies on the real ξ axis between -1 and $+1$, again assuming λ real, and using the notation of Eqs. (A24) and (A26),

$$\begin{aligned} &\operatorname*{Res}_{\xi\to\xi_b} \tfrac{1}{2}(\xi^{-2}-1) q_n^{+l} p_{n'}^l \\ &\quad = 2\pi i \operatorname*{Res}_{x\to x_b} \rho_l p_n^l p_{n'}^l \\ &\quad = -2T^{-1} w_l [2T\tau/(\tau^2 - T^2)]^2 p_n^l p_{n'}^l \,|_{T=n_b}\,. \end{aligned} \tag{B3}$$

To determine when a pole appears at the center of the circle, use Eqs. (A8) and (A17) in the limits of $\xi \to 0$, i.e., $T = \tau$, giving

$$\frac{q_n^{+l}p_{n'}^l}{2\xi^2}=-\frac{(n+2l+1)!\Gamma(n'+l+1-\tau)}{(n+1)!\Gamma(n+l+2-\tau)}\times(-\xi)^{n-n'-1}[1+O(\xi^2)]\ \text{as}\ \xi\to 0\ . \tag{B4}$$

Since $n\geq n'$ was assumed, a pole occurs only when $n=n'$, barring a complication when $\tau-l$ is a positive integer, to be treated as a special case below.

The sum of all the residues gives

$$I_{nn'}^l=\sum_{n_b=l+1}^{\infty}2\pi i\ \operatorname*{Res}_{x\to x_b}\rho_l p_n^l(x_b)p_{n'}^l(x_b)+\delta_{nn'}(n+1)_{2l+1}/(n+l+1-\tau)\ , \tag{B5}$$

thus affording the desired orthogonality relation

$$\oint d\rho_l p_n^l p_{n'}^l=\delta_{nn'}(n+1)_{2l+1}/(n+l+1-\tau)\ , \tag{B6}$$

where $d\rho_l$ is a weight function of the Stieltjes sort, taking jumps of $-2\pi i\,\mathrm{Res}\rho_l$ at each bound state and rising monotonically from $x=-1$ to $x=1$. This requires some stretching of the Stieltjes concept, however, since the jumps in $d\rho_l$ at the first few bound states as long as $n_b<\tau$ are negative resulting in negative orthogonality factors in Eq. (B6) for $n+l+1<\tau$. The cautious reader can check with the help of Appendix A that the terms in the sum in Eq. (B6) become $O(n_b^{-3})$ as n_b gets large, causing the sum to converge.

The very useful special case when $\tau=n_r+l+1$, where n_r+1 is a positive integer, causes some trouble by planting the bound-state pole for $n_b=\tau$ on top of the orthogonality pole at $\xi=0$. This modifies Eq. (B6) to

$$\oint' d\rho_l p_n^l p_{n'}^l=\begin{cases}\delta_{nn'}(n+1)_{2l+1}/(n+l+1-\tau) & \text{if } n,n'\neq n_r\\ (n_r+1)_{2l+1}/2\tau & \text{if } n=n_r \text{ and } n'=n_r\\ (n_r+1)_{2l+2}/2\tau & \text{if } n=n_r+1 \text{ and } n'=n_r\\ -(n_r)_{2l+2}/2\tau & \text{if } n=n_r \text{ and } n'=n_r-1\ ,\end{cases} \tag{B7}$$

where $\sum'$ indicates omission of $n_b=\tau$ in the sum. The deviations from orthogonality in Eq. (B7) could be foreseen from the linear dependence of $p_{n_r+1}^l$, $p_{n_r}^l$, and $p_{n_r-1}^l$ when the coefficient of x vanishes in Eq. (A10) at $\tau=n_r+l+1$. Moreover, this choice of τ sends what was a zero of each p_n^l for $n>n_r$ off to $x\to\infty$ ($\xi=0$), thereby reducing the degree of the polynomial. Hence, simply omitting $p_{n_r}^l$ from the set of polynomials gives an orthogonal set.

[1]P. G. Burke, D. F. Gallaher, and S. Geltman, J. Phys. B 2, 1142 (1969); P. G. Burke and J. F. B. Mitchell, *ibid.* 6, 320 (1973); P. G. Burke, K. A. Berrington, and C. V. Sukumar, *ibid.* 14, 289 (1981); N. Abu-Salbi and J. Callaway, Phys. Rev. A 24, 2372 (1981).

[2]A. U. Hazi and H. S. Taylor, Phys. Rev. A 1, 1109 (1970).

[3]C. W. McCurdy and J. F. McNutt, Chem. Phys. Lett. 94, 306 (1983).

[4]J. T. Broad, Phys. Rev. A 18, 1012 (1978).

[5]J. T. Broad, Phys. Rev. A 26, 3078 (1982).

[6]J. T. Broad, in *Electron-Atom and Electron-Molecule Collisions,* edited by J. Hinze (Plenum, London, 1983).

[7]E. J. Heller, W. P. Reinhardt, and H. A. Yamani, J. Comput. Phys. 13, 536 (1973).

[8]W. P. Reinhardt, Comput. Phys. Commun. 17, 1 (1979).

[9]H. A. Yamani and W. P. Reinhardt, Phys. Rev. A 11, 1144 (1975).

[10]E. J. Heller, T. N. Rescigno, and W. P. Reinhardt, Phys. Rev. A 8, 2946 (1973).

[11]P. W. Langhoff, in *Electron-Molecule and Photon-Molecule Collisions,* edited by T. N. Rescigno, V. McKoy, and B. Schneider (Plenum, New York, 1979).

[12]C. Cerjan, R. Hedges, C. Holt, W. P. Reinhardt, K. Scheibner, and J. J. Wendolski, Int. J. Quantum Chem. XIV, 393 (1978); S.-I Chu and W. P. Reinhardt, Phys. Rev. Lett. 39, 1195 (1977); A. Maquet, S.-I Chu, and W. P. Reinhardt, Phys. Rev. A 27, 2946 (1983).

[13]B. R. Junker, Int. J. Quantum Chem. XIV, 371 (1978); J. Turner and C. W. McCurdy, Chem. Phys. 71, 127 (1982).

[14]C. W. McCurdy and T. N. Rescigno, Phys. Rev. A 21, 1499 (1980); W. P. Reinhardt, Annu. Rev. Phys. Chem. (1982).

[15]B. R. Johnson and W. P. Reinhardt, Phys. Rev. A 28, 1930 (1983).

[16]A. Tip, J. Phys. A 16, 3237 (1983).

[17]M. Reed and B. Simon, *Methods of Modern Mathematical Physics* (Academic, New York, 1978), Vol. 4.

[18]J. Nuttall, Int. J. Quantum Chem. XIV, 519 (1978).

[19]M. Rittby, N. Elander, and E. Brandäs, Mol. Phys. 45, 553 (1982); E. Brandäs, P. Froelich, and M. Hehenberger, Int. J. Quantum Chem. XIV, 419 (1978).

[20]A. Grossmann and A. Tip, J. Phys. A 13, 3381 (1980).

[21]E. J. Heller and H. A. Yamani, Phys. Rev. A 9, 1201 (1974); 9, 1209 (1974); E. J. Heller, Phys. Rev. A 12, 1222 (1975); H. A. Yamani and L. Fishman, J. Math. Phys. 16, 410 (1975).

[22]D. K. Watson, R. R. Lucchese, V. McKoy, and T. N. Rescigno, Phys. Rev. A 21, 738 (1980).

[23]M. Aymar and M. Crance, J. Phys. B 13, L287 (1980).

[24]Y. Gontier, M. Poirer, and M. Trahin, J. Phys. B 13, 1381 (1980).

[25]C. R. Holt and W. P. Reinhardt, Phys. Rev. A 27, 2971 (1983).

[26]S. Klarsfeld and A. Maquet, J. Phys. B 12, L553 (1979); Phys. Lett. 73A, 100 (1979).

[27]H. A. Bethe and E. E. Salpeter, in *Handbuch der Physik,* edited by S. Flügge (Springer, Berlin, 1957), Vol. XXXV.

[28]L. Davidovich and H. M. Nussenzveig, in *Foundations of Radiation Theory and Quantum Electrodynamics,* edited by A. O. Barut (Plenum, New York, 1980).

[29]G. W. Erickson and D. R. Yennie, Ann. Phys. (N.Y.) 35, 271 (1965).

[30]S. Klarsfeld and A. Maquet, Phys. Lett. 43B, 201 (1973).

[31]A. Maquet, Phys. Rev. A 15, 1088 (1977).

[32]*Higher Transcendental Functions,* edited by A. Erdelyi (McGraw-Hill, New York, 1953).
[33]F. Pollaczek, C. R. Acad. Sci. **228**, 1363 (1949); **228**, 1998 (1949).
[34]G. A. Baker and P. R. Graves-Morris, *Padé Approximants: Basic Theory, Part I,* Vol. 13 of *Encyclopedia of Mathematics and its Applications,* edited by G. C. Rota (Addison-Wesley, New York, 1981).
[35]R. Loudon, *The Quantum Theory of Light* (Clarendon, Oxford, 1973).
[36]A. Messiah, *Quantum Mechanics* (North-Holland, Amsterdam, 1961).
[37]A. Poquérusse, Phys. Lett. **82A**, 232 (1981).
[38]M. J. Seaton, Proc. Phys. Soc. London **88**, 801 (1966); **88**, 815 (1966); J. Dubau and M. J. Seaton, J. Phys. B **17**, 381 (1984).
[39]P. Kruit, J. Kimman, H. G. Muller, and M. J. van der Wiel, Phys. Rev. A **28**, 248 (1983).
[40]H. G. Muller, A. Tip, and M. J. van der Wiel (unpublished); H. G. Muller and A. Tip (unpublished).
[41]R. G. Newton, *Scattering Theory of Waves and Particles* (McGraw-Hill, New York, 1966).
[42]M. Rotenberg, Adv. At. Mol. Phys. **6** (1970).
[43]L. Berg, *Asymptotische Darstellungen und Entwicklungen* (Deutsche Verlag der Wissenschaften, Berlin, 1968).
[44]Y. L. Luke, *The Special Functions and Their Applications* (Academic, New York, 1969).
[45]J. D. Wilkinson, *The Algebraic Eigenvalue Problem* (Oxford University, Oxford, 1965).
[46]G. Szegö, Proc. Am. Math. Soc. **1**, 731 (1950); J. A. Wilson, SIAM J. Math. Anal. **11**, 690 (1980).